Theoretical, Thermodynamic, Spectroscopic, and Structural Studies of the Consequences of One-Electron Oxidation on the Fe–X Bonds in 17- and 18-Electron Cp*Fe(dppe)X Complexes (X = F, Cl, Br, I, H, CH₃)

Mats Tilset,*,[1a,b] Irene Fjeldahl,[1b] Jean-René Hamon,*,[1c] Paul Hamon,[1c] Loïc Toupet,[1d] Jean-Yves Saillard,*,[1e] Karine Costuas,[1e] and Anthony Haynes[1f]

Contribution from the Department of Chemistry, University of Oslo, P.O. Box 1033, Blindern, N-0315 Oslo, Norway, UMR CNRS 6509, Organométalliques et Catalyse: Chimie et Electrochimie Moléculaires, Institut de Chimie de Rennes, Université de Rennes 1, Campus de Beaulieu, F-35042 Rennes Cedex, France, UMR CNRS 6626, Groupe Matière Condensée et Matériaux, Université de Rennes 1, Campus de Beaulieu, F-35042 Rennes Cedex, France, UMR CNRS 6511, Chimie du Solide et Inorganique Moléculaire, Institut de Chimie de Rennes, Université de Rennes 1, Campus de Beaulieu, F-35042 Rennes Cedex, France, and Department of Chemistry, University of Sheffield, Sheffield S3 7HF, England

Received March 15, 2001

Abstract: The compounds Cp*Fe(dppe)X ([Fe*]X) and the corresponding cation radicals [Fe*]X$^{•+}$ are available for the series X = F, Cl, Br, I, H, CH₃. This has allowed for a detailed investigation of the dependence of the nature of Fe–X bonding on the identity of X and the oxidation state (charge) of the complex. Cyclic voltammetry demonstrates that the electrode potentials for the [Fe*]X$^{0/+}$ couples decrease in the order I > Br > Cl > H > F > CH₃. An "inverse halide order" is seen, in which the most electronegative X leads to the most easily oxidized complex. This suggests that F is the *best donor* among the halides. The halide trend is also reflected in NMR spectroscopic data. Mössbauer spectroscopy data also suggest that the F ligand is a strong donor (relative to H and CH₃) in [Fe*]X$^{•+}$. DFT calculations on CpFe(dpe)X ([Fe]X) model complexes nicely reproduce the trend in the electrode potentials for the [Fe*]X$^{0/+}$ couples. Analysis of the theoretical data within the halogen series indicates that the energy of the [Fe]X HOMO does not correlate with the extent of its Fe(d_π)–X(p_π) antibonding character, which varies in the order I > Br > Cl > F, but rather depends on the destabilizing electrostatic effect caused by X. This effect varies in the order F > Cl > Br > I. A thermochemical cycle that incorporates the [Fe*]X$^{0/+}$ and [Fe*]$^{0/+}$ electrode potentials was used to investigate the effect of the oxidation state of the complex on the homolytic bond dissociation energy (BDE$_{hom}$), defined for the processes Fe–X → Fe$^•$ + X$^•$ and Fe–X$^{•+}$ → Fe^{+} + X$^•$. For all X, it was found that a one-electron oxidation leads to a *weakening* of the Fe–X bond. This trend was reproduced by the DFT calculations. On the other hand, IR $\nu_{Fe–X}$ spectroscopy data showed an increase in the stretching frequencies for X = H and Cl upon oxidation. X-ray crystallographic data showed a shortening of the Fe–Cl bond upon oxidation. The trends in IR and Fe–Cl bond distances were reproduced in the DFT calculations. The combined data therefore suggest that oxidation leads to weaker, but shorter, Fe–X bonds. A second thermochemical cycle was applied to investigate the effect of the one-electron oxidation on the heterolytic bond dissociation energies (BDE$_{het}$), defined for the processes Fe–X → Fe$^+$ + X$^-$ and Fe–X$^{•+}$ → Fe^{2+} + X$^-$. In this case, the oxidation led to bond *strengthening* in all cases. The computed BDE values have been analyzed within Ziegler's transition state methodology and decomposed into two components, one electrostatic and one covalent, describing the interaction between the unrelaxed fragments. In all the computed BDE$_{hom}$ and BDE$_{het}$ values of the [Fe]X models the electrostatic component is important. This helps to understand their respective variations upon oxidation.

Introduction

Knowledge of the nature and energetics of metal–ligand bonding in organotransition-metal complexes is crucial to the understanding of organometallic reactions and catalysis.[2] Insight into the often complex reaction mechanisms based on a quantitative understanding of strengths of bonds being formed and broken in the reaction steps that are involved may ultimately help in the design of new and improved processes.

Recently, the nature of the bonding between organotransition-metal centers and electronegative σ-bonded ligands X such as halide, alkoxide, and amido groups has received considerable attention.[3] In addition to forming covalent M–X bonds, these ligands are capable of acting as π donors toward the metal. A

(1) (a) Corresponding author. E-mail: mats.tilset@kjemi.uio.no. (b) University of Oslo. (c) UMR CNRS 6509, Université de Rennes 1. (d) UMR CNRS 6626, Université de Rennes 1. (e) UMR CNRS 6511, Université de Rennes 1. (f) University of Sheffield.
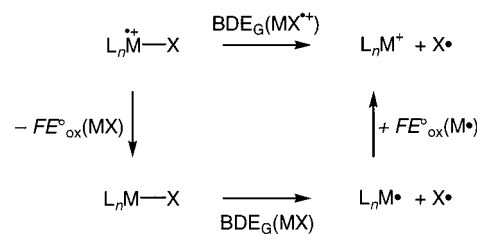
(2) (a) Simões, J. A. M.; Beauchamp, J. L. *Chem. Rev.* **1990**, *90*, 629. (b) Simões, J. A. M., Ed. *Energetics of Organometallic Species*; Kluwer Academic: Dordrecht, The Netherlands, 1992. (c) Marks, T. J., Ed. *Bonding Energetics in Organometallic Compounds*; ACS Symp. Ser. No. 428; American Chemical Society: Washington, DC, 1990. (d) Halpern, J. *Inorg. Chim. Acta* **1985**, *100*, 41. (e) Minas da Piedade, M. E., Ed. *Energetics of Stable Molecules and Reactive Intermediates*; Kluwer Academic: Dordrecht, The Netherlands, 1999.

ligand p_π−metal d_π electron-pair interaction generally serves to destabilize electronically saturated complexes via filled−filled repulsive interactions, whereas coordinatively unsaturated species may achieve considerable stabilization through partial π bond formation.[4] A substantial line of evidence,[3] including IR ν_{CO} spectroscopy data,[5,6] electrode potentials,[7] chemical reactivity,[5,8] and theoretical calculations,[4b,5a,9] suggests that among the halides, it is the fluoride ligand that appears to be the most efficient electron-pair donor toward the metal. The nature of this interaction, at least in saturated complexes, remains highly controversial, however: Holland et al.[10] have provided an alternative explanation based on Drago's $E−C$ bonding scheme.[11] Here, M−X bonding is primarily explained in terms of electrostatic (E) and covalent (C) contributions. Destabilizing π interactions were considered not to be the major source of M−X bonding preferences in some late metal complexes.[10]

The presence of significant π bonding from halide to metal should be reflected in bond dissociation energy (BDE) changes when this bonding is "switched on"[4a] by the generation of coordinative unsaturation. The unsaturation can conceptually be generated by ligand dissociation from 18-electron precursors or by two-electron oxidations of the 18-electron species. One might even expect "partial unsaturation" to be achieved by one-electron oxidations. With this in mind, we have investigated the effects of one- and two-electron oxidation processes on M−X bonding through the use of thermochemical cycles that incorporate electrode potential data. Such techniques have proven powerful for extracting bond energy data that are frequently not directly available by other experimental methods. Transient electrochemical techniques, of which cyclic voltammetry is most commonly used, offer the advantage that relatively short-lived species can be investigated. The methodology was pioneered in organic chemistry by Breslow and co-workers[12] and was later adapted by numerous research groups, as manifested by a number of relevant reviews.[13]

During the past decade, analogous thermochemical cycles have been adapted to investigate M−H bonding energetics in

(3) For recent reviews, see: (a) Caulton, K. G. *New J. Chem.* **1994**, *18*, 25. (b) Doherty, N. M.; Hoffman, N. W. *Chem. Rev.* **1991**, *91*, 553.

(4) (a) Poulton, J. T.; Folting, K.; Streib, W. E.; Caulton, K. G. *Inorg. Chem.* **1992**, *31*, 3190. (b) Johnson, T. J.; Folting, K.; Streib, W. E.; Eisenstein, O.; Caulton, K. G. *Inorg. Chem.* **1995**, *34*, 488. (c) Bickford, C. C.; Johnson, T. J.; Davidson, E. R.; Caulton, K. G. *Inorg. Chem.* **1994**, *33*, 1080. (d) Barthazy, P.; Stoop, R. M.; Wörle, M.; Togni, A.; Mezzetti, A. *Organometallics* **2000**, *19*, 2844.

(5) (a) Poulton, J. T.; Sigalas, M. P.; Folting, K.; Streib, W. E.; Eisenstein, O.; Caulton, K. G. *Inorg. Chem.* **1994**, *33*, 1476. (b) Huang, D. J.; Caulton K. G. *J. Am. Chem. Soc.* **1997**, *119*, 3185.

(6) Vaska, L.; Peone, J. *J. Chem. Soc., Chem. Commun.* **1971**, 418.

(7) Schiavon, G.; Zecchin, S.; Pilloni, G.; Martelli, M. *Inorg. Nucl. Chem.* **1977**, *39*, 115.

(8) Darensbourg, D. J.; Klausmeyer, K. K.; Reibenspies, J. H. *Inorg. Chem.* **1995**, *34*, 4933.

(9) Abu-Hassayan, F.; Goldman, A. S.; Krogh-Jespersen, K. *Inorg. Chem.* **1994**, *33*, 5122.

(10) (a) Holland, P. L.; Andersen, R. A.; Bergman, R. G.; Huang, J.; Nolan, S. P. *J. Am. Chem. Soc.* **1997**, *119*, 12800. (b) Holland, P. L.; Andersen, R. A.; Bergman, R. G. *Comments Inorg. Chem.* **1999**, *21*, 115.

(11) (a) Drago, R. S. *Applications of Electrostatic-Covalent Models in Chemistry*; Surfside: Gainesville, FL, 1994. (b) Drago, R. S.; Wong, N. M.; Ferris, D. C. *J. Am. Chem. Soc.* **1992**, *114*, 91.

(12) (a) Breslow, R.; Chu, W. *J. Am. Chem. Soc.* **1973**, *95*, 411. (b) Breslow, R.; Grant, J. *J. Am. Chem. Soc.* **1977**, *99*, 7745. (c) Jaun, B.; Schwarz, J.; Breslow, R. *J. Am. Chem. Soc.* **1980**, *102*, 5741.

(13) (a) Wayner, D. D. M.; Parker, V. D. *Acc. Chem. Res.* **1993**, *26*, 287. (b) Arnett, E. M.; Flowers, R. A.; Ludwig, R. T.; Meckhof, A.; Walek, S. *Pure Appl. Chem.* **1995**, *67*, 729. (c) Bordwell, F. G.; Satish, A. V.; Zhang, S.; Zhang, X.-M. *Pure Appl. Chem.* **1995**, *67*, 735. (d) Arnett, E. M.; Flowers, R. A. *Chem. Soc. Rev.* **1993**, *22*, 9. (e) Bordwell, F. G.; Zhang, X.-M. *Acc. Chem. Res.* **1993**, *26*, 510. (f) Astruc, D. *Acc. Chem. Res.* **2000**, *33*, 287.

Scheme 1

organotransition-metal hydrides.[14,15] Absolute homolytic M−H bond dissociation energies (henceforth to be denoted BDE_{hom}) in solution have been determined, and relative M−H acidity (pK_a) and BDE_{hom} data for 18-electron neutral complexes and their 17-electron cation radicals have been estimated. The method that was applied to evaluate the M−H BDE differences between 18- and 17-electron species[14c,d] can be straightforwardly modified to accommodate any M−X bond. Scheme 1 depicts the resulting thermochemical cycle that can be used to evaluate the effect of a one-electron oxidation on the homolytic M−X bond dissociation energy through eq 1 . (The subscript "G" in

$$\Delta BDE_{hom} = BDE_{hom}(MX^{\bullet+}) - BDE_{hom}(MX) =$$
$$F[E^\circ_{ox}(M^\bullet) - E^\circ_{ox}(MX)] \quad (1)$$

the scheme signifies that the quantities are Gibbs free energy changes; enthalpy values may be obtained if the entropy contributions from the two redox couples cancel. This may be assumed to be the case for large molecules of similar shapes and charges,[16] as will be the case in this work). Thus, according to eq 1, BDE changes between 18-electron M−X and 17-electron M−X$^{\bullet+}$ can be determined if electrode potentials for the M−X/M−X$^+$ and M$^\bullet$/M$^+$ couples are available.

Data pertaining to the consequences of one-electron oxidations on M−X bonding in organotransition-metal complexes are scarce. Past results from our laboratories[14c,d] have established that one-electron oxidations of low-oxidation state metal carbonyl hydrides ($CpCr(CO)_2(L)H$, where L = $P(OMe)_3$, PPh_3, PEt_3; $Cp*Cr(CO)_3H$; and $TpM(CO)_3H$ and $Tp*M(CO)_3H$, where M = Cr, Mo, W)[17] consistently cause M−H BDE values to be reduced by ca. 30 kJ/mol. Contrasting these results, the IR $\nu_{Fe−H}$ stretching frequency was raised from 1869 to 1886 cm^{-1}, indicative of a strengthened Fe−X bond, when $Cp*Fe(dppe)H$ was oxidized to its stable cation radical.[18,19] Shifts to higher energies are also observed in the Cp′Fe(dippe)H$^{0/+}$ series (Cp′

(14) (a) Tilset, M.; Parker, V. D. *J. Am. Chem. Soc.* **1989**, *111*, 6711; **1990**, *112*, 2843 (corrigendum). (b) Parker, V. D.; Handoo, K. L.; Roness, F.; Tilset, M. *J. Am. Chem. Soc.* **1991**, *113*, 7493. (c) Tilset, M. *J. Am. Chem. Soc.* **1992**, *114*, 2740. (d) Skagestad, V.; Tilset, M. *J. Am. Chem. Soc.* **1993**, *115*, 5077. (e) Pedersen, A.; Skagestad, V.; Tilset, M. *Acta Chem. Scand.* **1995**, *49*, 632.

(15) (a) Berning, D. E.; Noll, B. C.; DuBois, D. L. *J. Am. Chem. Soc.* **1999**, *121*, 11432. (b) Berning, D. E.; Miedaner, A.; Curtis, C. J.; Noll, B. C.; DuBois, M. C. R.; DuBois, D. L. *Organometallics* **2001**, *20*, 1832.

(16) The assumption has been found to hold well for organic radicals R$^\bullet$ vs hydrocarbons R−H: Wayner, D. D. M.; McPhee, D. J.; Griller, D. *J. Am. Chem. Soc.* **1988**, *110*, 132.

(17) Abbreviations: Cp = η^5-C$_5$H$_5$; Cp* = η^5-C$_5$Me$_5$; dppe = η^2-Ph$_2$PCH$_2$CH$_2$PPh$_2$; dpe = η^2-H$_2$PCH$_2$CH$_2$PH$_2$; dippe = η^2-^{i}Pr$_2$PCH$_2$CH$_2$P^{i}Pr$_2$; BАr$_f^-$ = [3, 5-(CF$_3$)$_2$C$_6$H$_3$]$_4$B$^-$; Tp = HB(C$_3$H$_3$N$_2$)$_3$; Tp* = HB(3,5-Me$_2$C$_3$-HN$_2$)$_3$; [Fe*] = Cp*Fe(dppe); [Fe] = CpFe(dpe).

(18) The previous report (ref 19) of a *lower-energy shift* from 1869 to 1860 cm^{-1} upon oxidation was based on erroneous data for the cation. Reproducible data have now been obtained from different batches of **5**$^+$PF$_6^-$ (see Experimental Section).

(19) (a) Roger, C.; Hamon, P.; Toupet, L.; Rabaâ, H.; Saillard, J.-Y.; Hamon, J.-R.; Lapinte, C. *Organometallics* **1991**, *10*, 1045. (b) Hamon, P.; Toupet, L.; Hamon, J.-R.; Lapinte, C. *Organometallics* **1992**, *11*, 1429.

= Cp, 1911 vs 1939 cm^{-1}; Cp' = Cp*, 1901 vs 1915 cm^{-1}).[20] Poli and co-workers[21] recently reported that the IR ν_{M-H} stretching frequencies of Cp*M(dppe)H$_3$$^{•+}$ (M = Mo, W) were 10−20 cm^{-1} higher than those for the neutral counterparts. These IR results indicate an oxidative strengthening of the M−H bonds also in the relatively high oxidation state complexes, and this conclusion was supported by DFT calculations for the Cp*W(dppe)H$_3$$^{0/+}$ system. Finally, IR ν_{M-H} data have been reported for redox couples of non-Cp hydridometal phosphine complexes of Co[22] and W;[23] oxidation-induced frequency shifts occur to higher and lower frequencies in these systems.

It has been demonstrated that the sterically crowded and electron-rich Cp*Fe(dppe) moiety[24] (to be abbreviated as [Fe*]) supports metal complexes in a great number of oxidation states, and compounds have been isolated with electron counts ranging from 16 to 19.[19,25] A persistent 15-electron species has even been generated in solution.[25e] The Cp*Fe(dppe) derivatives therefore are particularly well suited for the application of thermochemical cycles. In this contribution, we probe the details of Fe−X bonding in a range of Cp*Fe(dppe)X complexes (X = F, Cl, Br, I, H, CH$_3$) using a variety of techniques, including electrochemistry, thermochemical cycles, X-ray structural studies, NMR, IR, ESR, and Mössbauer spectroscopy, as well as theoretical (DFT) calculations. Parts of the experimental results have been previously communicated.[26]

Results and Discussion

I. Preparation of Complexes and Structural and Spectroscopic Studies. The preparative work was aimed at complementing a family of related complexes of the type Cp*Fe(dppe)-X^{n+} [X = F (**1**), Cl (**2**), Br (**3**), I (**4**), H (**5**), Me (**6**)] with a variety of σ-bonded X ligands, both as 18-electron neutral species (*n* = 0) and as 17-electron radical cations (*n* = 1). This has facilitated a detailed investigation on the effect of X on spectroscopic and electrochemical properties and on Fe−X bonding energetics in this series of complexes.

Synthesis of the Iron(II) Halide Complexes. The novel fluoro complex Cp*Fe(dppe)F (**1**) is prepared in almost quantitative isolated yield (86%) by treating the paramagnetic, red 16-electron Cp*Fe(dppe)$^+$PF$_6$$^-$ derivative[25e] with 1 equiv of dry CsF in THF (Scheme 2). Complex **1** is isolated as a thermally stable, yellowish-green powder, and can be stored for several weeks under argon without any signs of decomposition. This first isolated organometallic Fe(II) fluoride compound bearing a cyclic hydrocarbon ligand[27] proved to be rather sensitive in solution and all attempts at recrystallizing it failed,

(20) Jimenez-Tenorio, M.; Puerta, M. C.; Valerga, P. *Organometallics* **1994**, *13*, 3330.

(21) Pleune, B.; Morales, D.; Meunier-Prest, R.; Richard, P.; Collange, E.; Fettinger, J. C.; Poli, R. *J. Am. Chem. Soc.* **1999**, *121*, 2209.

(22) (a) Pilloni, G.; Schiavon, G.; Zotti, G.; Zecchin, S. *J. Organomet. Chem.* **1977**, *134*, 305. (b) Bianchini, C.; Innocenti, P.; Meli, A.; Peruzzini, M.; Zanobini, F.; Zanello, P. *Organometallics* **1990**, *9*, 2514. (c) Kruse, W.; Atalla, J. H. *Chem. Commun.* **1968**, 921. (d) Sacco, A.; Ugo, R. *J. Chem. Soc.* **1964**, 3274. (e) Ghilardi, C. A.; Midollini, S.; Sacconi, L. *Inorg. Chem.* **1975**, *14*, 1790.

(23) Sharp, P. R.; Frank, K. G. *Inorg. Chem.* **1985**, *24*, 1808.

(24) Paul, F.; Lapinte, C. *Coord. Chem. Rev.* **1998**, *178−180*, 427.

(25) (a) Roger, C.; Marseille, P.; Salus, C.; Hamon, J.-R.; Lapinte, C. *J. Organomet. Chem.* **1987**, *336*, C13. (b) Morrow, J.; Catheline, D.; Desbois, M.-H.; Manriquez, J. M.; Ruiz, J.; Astruc, D. *Organometallics* **1987**, *6*, 2605. (c) Morrow, J. R.; Astruc, D. *Bull. Soc. Chim. Fr.* **1992**, *129*, 319. (d) Hamon, P.; Hamon, J.-R.; Lapinte, C. *J. Chem. Soc., Chem. Commun.* **1992**, 1602. (e) Hamon, P.; Toupet, L.; Hamon, J.-R.; Lapinte, C. *Organometallics* **1996**, *15*, 10.

(26) Tilset, M.; Hamon, J.-R.; Hamon, P. *Chem. Commun.* **1998**, 765.

(27) Murphy, E. F.; Murugavel, R.; Roesky, H. W. *Chem. Rev.* **1997**, *97*, 3425.
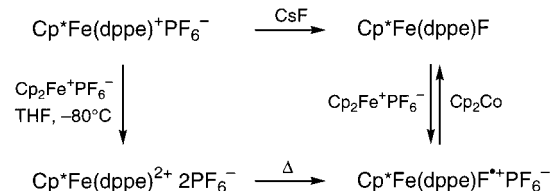
Scheme 2

Table 1. Selected NMR Chemical Shift Data for Neutral Cp*Fe(dppe)X Complexes^a

compound	^{1}H (C$_5$Me$_5$)	^{13}C{^{1}H} (C$_5$*Me$_5$*)	^{13}C{^{1}H} (*C$_5$*Me$_5$)	^{31}P (dppe)
Cp*Fe(dppe)F (**1**)	1.33	10.0	82.9	89.4
Cp*Fe(dppe)Cl (**2**)	1.40	10.3	83.6	91.6
Cp*Fe(dppe)Br (**3**)	1.53	10.8	83.6	93.2
Cp*Fe(dppe)I (**4**)	1.61	11.5	83.6	95.1
Cp*Fe(dppe)H (**5**)	1.62	11.5	85.2	107.9
Cp*Fe(dppe)Me (**6**)	1.47	10.5	85.5	106.5

^{a} Chemical shifts (δ) recorded in benzene-d_6 at ambient temperature.

leading always to decomposition to unidentified products. Consequently, neither satisfactory elemental analysis nor crystals suitable for an X-ray structural determination could be obtained. Analogous relative instabilities of low oxidation state, coordinatively saturated Fe^{28a} and Mo^{28b} fluoro complexes have been recently reported, and also in those cases precluded their isolation. Analytically pure CpRe(PPh$_3$)(NO)F can be isolated but decomposes on the time scale of hours in solution.[29] Despite this instability in solution, complex **1** features good ^{1}H, ^{13}C, ^{31}P, and ^{19}F NMR spectra (see Experimental Section and Table 1) that were obtained from a sample that was analyzed by NMR immediately after its preparation. The presence of the fluoride as the sixth ligand in **1** is clearly authenticated by a doublet at δ 89.4 in the ^{31}P NMR spectrum and a triplet at δ −44.4 in the ^{19}F NMR spectrum ($^2J_{PF}$ = 43 Hz). Similarly, large couplings between P and F bonded to the same metal center are commonly observed for metal phosphine fluorides.[3b,4d,29−31] The cyclic voltammogram of complex **1** (vide infra) exhibits two reversible, monoelectronic waves attributable to a single redox-active species.

The neutral Fe(II) bromo complex Cp*Fe(dppe)Br (**3**) is readily prepared by chloride−bromide ion exchange between the known Cp*Fe(dppe)Cl (**2**) and KBr in dichloromethane, following the same procedure as that previously described for the iodo derivative Cp*Fe(dppe)I (**4**).[19a] The complex **3** was isolated in 90% yield after slow crystallization, as air and thermally stable, dark-brown crystals that provided satisfactory elemental analysis.

Table 1 summarizes some key NMR data, recorded under identical conditions, for the series **1**−**6**. In several respects, fluoro complex **1** stands out from the other halides. For example, the ^{1}H signal of the Cp* ligand at δ 1.33 and the dppe ^{31}P NMR signal at δ 89.4 appear substantially upfield shifted relative to the others (δ 1.40−1.61 and 91.6−95.1, respectively). In fact, there is a general trend in the data in Table 1 that the chemical shift decreases with increasing halide electronegativity. This trend is opposite to that reported by Gladysz et al. for the CpRe-(PPh$_3$)(NO)X series,[29] and also counters the trend that might

(28) (a) Landau, S. E.; Morris, R. H.; Lough, A. J. *Inorg. Chem.* **1999**, *38*, 6060. (b) Aston, G. M.; Badriya, S.; Farley, R. D.; Grime, R. W.; Ledger, S. J.; Mabbs, F. E.; McInnes, E. J. L.; Morris, H. W.; Ricalton, A.; Rowlands, C. C.; Wagner, K.; Whiteley, M. W. *J. Chem. Soc., Dalton Trans.* **1999**, 4379.

(29) Agbossou, S. K.; Roger, C.; Igau, A.; Gladysz, J. A. *Inorg. Chem.* **1992**, *31*, 419.

be anticipated on the basis of the relative electronegativities of the halide ligands. However, the trend is in good agreement with the electrochemical data (vide infra): The more electron rich complex exhibits the most upfield shifted NMR signals.

The instability of complex **1** may not be too surprising if one considers the generalized perturbation theory of donor−acceptor interactions, which does not favor the formation of a stable covalent Fe−F bond.[32] As predicted by the "hard and soft acid and base" (HSAB) concept,[33] the interaction between F⁻, the hardest base known, and soft acids, such as the low-valent Fe center in Cp*Fe(dppe)⁺, should be weak. Soft acids are expected to exhibit considerably higher affinity for the heavier halide ions. However, this is not always true. For instance, several authors have clearly demonstrated that the order F⁻ > Cl⁻ > Br⁻ > I⁻ is characteristic of anion affinity for cationic, coordinatively unsaturated Rh(I),[34] Pd(II),[35] and W(II)[36] moieties in media of low polarity.

Chemical Oxidations: Synthesis of the 17-Electron Iron-(III) Halide Complexes. Cyclic voltammetric investigations (vide infra) revealed that **1**, **3**, and **4** all undergo reversible one-electron oxidations to the corresponding 17-electron radical cations. This is analogous to the behavior of **2**, **5**, and **6** that has been previously reported.[19] These oxidations occur at potentials that suggest the use of Cp₂Fe⁺ salts as chemical oxidants. Accordingly, PF₆⁻ salts of the 17-electron complexes Cp*Fe(dppe)X⁺ [X = F (**1**⁺), Br (**3**⁺), I (**4**⁺)] were synthesized by one-electron oxidations with 0.9 equiv of Cp₂Fe⁺PF₆⁻ in THF and were isolated as dark red (**1**⁺) or black (**3**⁺ and **4**⁺) microcrystals in 87, 95, and 90% yield, respectively. These air and thermally stable compounds exhibit cyclic voltammetry waves identical with those of their Fe(II) precursors. Accordingly, the cations can be chemically reduced with 1 equiv of Cp₂Co to quantitatively regenerate the respective 18-electron complexes.

Originally, the novel Fe(III) fluoro derivative **1**⁺PF₆⁻ was unexpectedly isolated in 81% yield as analytically pure dark red crystals from the reaction of the 16-electron cation Cp*Fe(dppe)⁺PF₆⁻ with Cp₂Fe⁺PF₆⁻ (Scheme 2). Based on the redox potentials determined by cyclic voltammetry (vide infra), the first step of the reaction is believed to be a one-electron oxidation to generate the dicationic 15-electron intermediate Cp*Fe(dppe)²⁺ that reacts via F⁻ abstraction from PF₆⁻ to provide the 17-electron fluoro complex **1**⁺PF₆⁻. PF₅ was not detected in this reaction but its formation was implicated by the observed polymerization of the THF solvent. The abstraction of fluoride from the PF₆⁻ anion in the above reaction is presumably a result of the potent Lewis acidity of the 5-coordinated metal dication intermediate Cp*Fe(dppe)²⁺. The half-sandwich complex CpMo(dppe)(MeCN)ClF⁺PF₆⁻, resulting from thermal decarbonylation of the 17-electron CpMo(CO)-
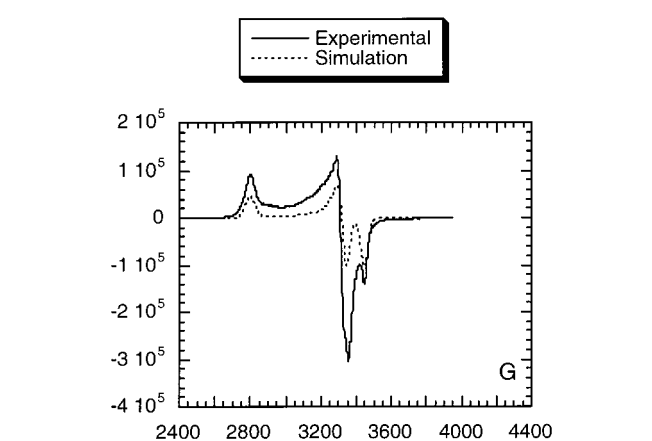

Figure 1. X-band ESR spectrum of Cp*Fe(dppe)F⁺PF₆⁻ (**1**⁺PF₆⁻) recorded on a 9:1 THF/pentane frozen solution (glass) at 77 K.

(dppe)Cl⁺PF₆⁻, is also believed to arise via a 15-electron intermediate CpMo(dppe)Cl⁺.[31]

The structures of these three new 17-electron Fe(III) halides were confirmed by elemental analysis, magnetic susceptibility measurements, and an X-ray crystal structure determination of **1**⁺PF₆⁻ (vide infra). The complexes **1**⁺PF₆⁻, **3**⁺PF₆⁻, and **4**⁺PF₆⁻ exhibit magnetic moments $\mu_{eff} = 1.9$, 2.7, and 2.3 μB, respectively, as determined in solution by Evans' method.[37] These values correspond reasonably well to a d⁵ low-spin configuration. As already noted for related 17-electron Fe(III) half-sandwich compounds, these magnetic moments are somewhat greater than the calculated spin-only value (1.73 μB) for one unpaired electron, and this has been attributed to orbital contributions.[19a]

A crystalline sample of the fluoro derivative **1**⁺PF₆⁻ was subjected to zero-field Mössbauer spectrometry at 80 K. The spectrum exhibits a single Mössbauer doublet with typical isomeric shift (IS) and quadrupole splitting (QS) parameters diagnostic of a pure d⁵ low-spin Fe(III) species.[19,24,25] In addition, both IS and QS parameters can provide insight into the nature of the bond to iron.[38] Moreover, in such half-sandwich 17-electron Fe(III) complexes, it has been noted that the IS value increases with the electron releasing power of the X group.[39] The high IS value of 0.426 mm/s vs Fe recorded for Cp*Fe(dppe)F⁺PF₆⁻ would therefore suggest that the fluoride acts as an apparently strong σ-donor ligand. The IS value is indeed greater than those measured for Cp*Fe(dppe)H⁺PF₆⁻ (0.260 mm/s) and Cp*Fe(dppe)Me⁺PF₆⁻ (0.35 mm/s).[19] It is also noteworthy that the QS value of 0.915 mm/s is also large compared to those of **5**⁺ (0.84) and of **6**⁺ (0.76).

The X-band ESR spectrum (Figure 1) of **1**⁺PF₆⁻ was recorded on a 9:1 THF/pentane frozen solution (glass) at 77 K. The spectrum displays three well-separated signals corresponding to the three g-tensor components, appropriate for a pseudooctahedral environment around the Fe-centered radical. The extrapolated values ($g_x = 2.419$, $g_y = 2.018$, $g_z = 1.998$) confirm the metal-centered radical nature of the 17-electron cationic species.[19,24] The g_y and g_z values are close to the free-electron g value (g = 2.0023), whereas the g_x component ($g_x = 2.419$) is much larger, as usually noted for such monomeric Fe(III)

(30) Veltheer, J. E.; Burger, P.; Bergman, R. G. *J. Am. Chem. Soc.* **1995**, *117*, 12478.

(31) Fettinger, J. C.; Keogh, D. W.; Poli, R. *J. Am. Chem. Soc.* **1996**, *118*, 3617.

(32) Klopman, G. In *Chemical Reactivity and Reaction Paths*; Klopman, G., Ed.; Wiley: New York, 1974; p 55.

(33) Pearson, R. G. In *Hard and Soft Acids and Bases*; Dowden, Hutchison and Ross: Stroudsburg, PA, 1973.

(34) (a) Branan, D. M.; Hoffman, N. W.; McElroy, E. A.; Miller, N. C.; Ramage, D. L.; Schott, A. F.; Young, S. H. *Inorg. Chem.* **1987**, *26*, 2915. (b) Araghizadeh, F.; Branan, D. M.; Hoffman, N. W.; Jones, J. H.; McElroy, E. A.; Miller, N. C.; Ramage, D. L.; Salazar, A. B.; Young, S. H. *Inorg. Chem.* **1987**, *26*, 3752.

(35) Flemming, J. P.; Pilon, M. C.; Borbulevitch, O. Y.; Antipin, M. Y.; Grushin, V. V. *Inorg. Chim. Acta* **1998**, *280*, 87.

(36) Bartlett, I. M.; Carlton, S.; Connelly, N. G.; Harding, D. J.; Hayward, O. D.; Orpen, A. G.; Ray, C. D.; Rieger, P. H. *Chem. Commun.* **1999**, 2403.

(37) (a) Evans, D. F. *J. Chem. Soc.* **1959**, 2003. (b) Crawford, T. H.; Swanson, J. *J. Chem. Educ.* **1971**, *48*, 382.

(38) Guillaume, V.; Thominot, P.; Coat, F.; Mari, A.; Lapinte, C. *J. Organomet. Chem.* **1998**, *565*, 75.

(39) Paul, F.; Meyer, W. E.; Toupet, L.; Jiao, H.; Gladysz, J. A.; Lapinte, C. *J. Am. Chem. Soc.* **2000**, *122*, 9405.

low-spin configuration compounds, indicating strong interactions between the single electron and the electrons of lower lying orbitals.[40] However, *the signal at high field* is weaker than usually observed.[24] Indeed, the simulation of the spectrum indicates that this signal corresponds to one line of the doublet resulting from the coupling of the unpaired electron to the ^{19}F nucleus ($A_F = 110$ G). The second line of this doublet overlaps with the g_y signal, for which a smaller coupling constant $A_F = 60$ G is estimated. These ESR data agree well with those reported for the d^3 tungsten derivative Tp*W(CO)(MeCCMe)-F$^{\bullet+}$, where the three hyperfine A_F coupling constants ($A_1 = 108$ G, $A_2 = 22$ G, $A_3 = 18$ G) have been estimated.[36] Hyperfine coupling with the phosphorus nuclei in 1^+ was not observed.

Infrared spectra of **5** and **5**$^+$PF$_6^-$ (Nujol mulls) revealed absorptions that are assigned to the ν_{Fe-H} stretching modes at 1869 and 1886 cm^{-1}, respectively.[18] Attempts were also made at locating the IR ν_{Fe-X} stretching vibrations for the halides. Spectra were run on both a dispersive instrument (see Experimental Section for details) in the region 600–200 cm^{-1} and an FTIR instrument with a cutoff at 400 cm^{-1}. Spectra were recorded for the whole series of neutral and cationic complexes except the unstable Cp*Fe(dppe)F complex. Absorptions that were common to all complexes within the neutral series were rejected on the grounds that they would likely originate from the Cp*Fe(dppe) moiety, rather than the Fe–X bond vibration, and similarly for the cationic series (which also displayed a common band at 557 cm^{-1} for the PF$_6^-$ counterion). Absorptions that could then with some confidence be attributed to the Fe–X stretching mode were found only for the Cp*Fe(dppe)Cl$^{0/+}$ (**2**$^{0/+}$) couple; unfortunately, the other halides did not provide useful data for our purpose. A band at 337 cm^{-1} assigned to the Fe–Cl stretching mode of **2** exhibited a shift to 367 cm^{-1} in **2**$^+$.[41] A very similar shift (from 349 to 373 cm^{-1}) was reported for the ν_{Fe-Cl} modes of an Fe(diarsine)$_2$Cl$_2^{0/+}$ couple.[42] The measured data for **2** and **2**$^+$ agree quite well with DFT calculated values of 279 and 307 cm^{-1}, respectively, for the model compounds CpFe(dpe)Cl and CpFe(dpe)Cl$^+$ (vide infra).

X-ray Crystal Structure Determinations of 1$^+$PF$_6^-$, 2$^+$PF$_6^-$, and 6$^+$BF$_4^-$. The crystal structures of compounds **1**$^+$PF$_6^-$, **2**$^+$PF$_6^-$, and **6**$^+$BF$_4^-$ have been determined as outlined in the Experimental Section. The molecular structures of the three cationic organometallic moieties **1**$^+$, **2**$^+$, and **6**$^+$ are presented in similar perspectives for the sake of comparison in Figure 2. Relevant interatomic distances and angles for the three complexes are listed in Table 2, together with key data[19a] for the related neutral chloro compound. In each species, the iron atom shows a pseudooctahedral coordination with the three-legged piano-stool geometry, and the three compounds exhibit general features that compare well with previous structures in this mononuclear Fe(III) σ-bonded Cp*Fe(dppe)X$^+$ series.[24,43,44]

Although some X-ray characterized mononuclear coordination[45,46] and purely inorganic[47] iron fluorides have been reported, to the best of our knowledge, the crystal structure of the fluoro compound **1**$^+$PF$_6^-$ is the first one to be reported for a molecular organometallic iron complex containing a fluoro ligand. In this

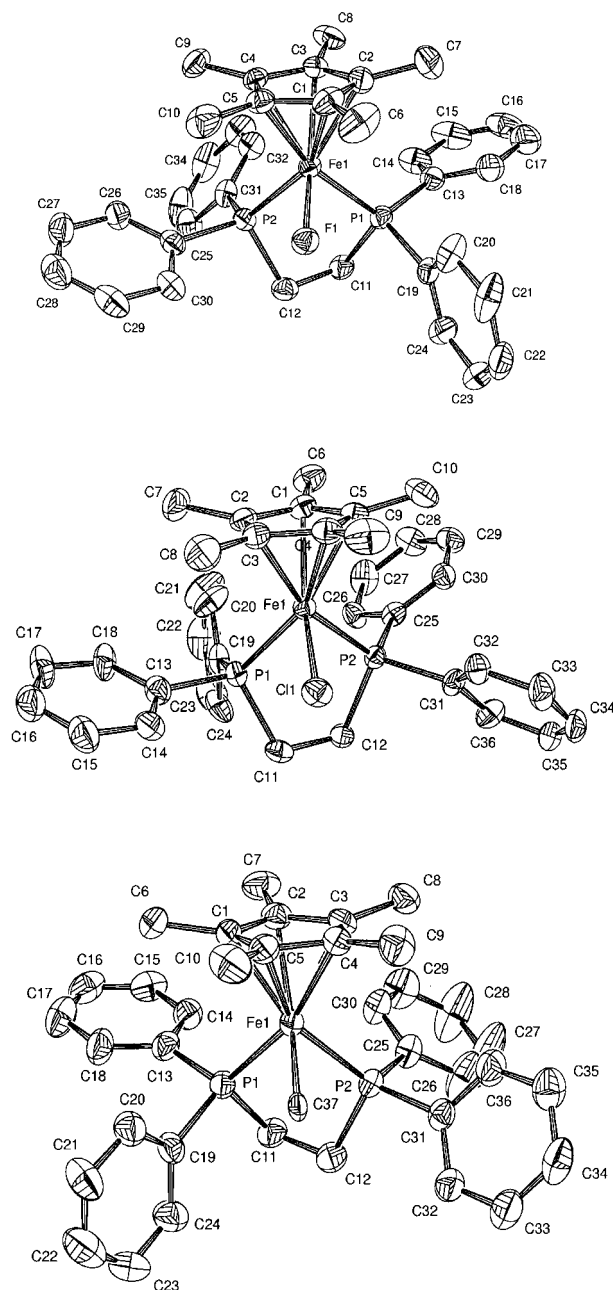**Figure 2.** ORTEP drawings of the cationic moieties of the X-ray structures of **1**$^+$PF$_6^-$ (top), **2**$^+$PF$_6^-$ (center), and **6**$^+$BF$_4^-$ (bottom). See Table 2 for selected bond lengths and angles and Table 11 for crystal data, data collection, and refinement parameters.

respect, the Fe–F distance deserves particular attention. The Fe–F bond length in **1**$^+$ might be compared with the Fe–Cl bond distance of 2.237(2) Å (Table 2) in the analogous compound **2**$^+$PF$_6^-$. This Fe–Cl bond distance and the difference

(40) Rieger, P. H. *Coord. Chem. Rev.* **1994**, *135–136*, 203.

(41) IR bands observed at 394, 426, and 436 cm^{-1} for **2** also exhibited shifts to 448, 475, and 483 cm^{-1}, respectively, for **2**$^+$. These bands are assigned to $\nu_{Fe-ligand}$ modes (predominantly ν_{Fe-P}), but we cannot rule out some mixing with the ν_{Fe-Cl} vibration.

(42) Lewis, J.; Nyholm, R. S.; Rodley, G. A. *J. Chem. Soc.* **1965**, 1483.

(43) Roger, C.; Toupet, L.; Lapinte, C. *J. Chem. Soc., Chem. Commun.* **1988**, 713.

(44) Denis, R.; Toupet, L.; Paul, F.; Lapinte, C. *Organometallics* **2000**, *19*, 4240.

(45) Hexacoordinated high-spin Fe(III) fluorides of the type Fe(porphyrin)F have been structurally characterized. (a) Anzai, K.; Hatano, K.; Lee, Y. J.; Scheidt, W. R. *Inorg. Chem.* **1981**, *20*, 2337. (b) Scheidt, W. R.; Lee, Y. J.; Tamai, S.; Hatano, K. *J. Am. Chem. Soc.* **1983**, *105*, 778. (c) Lee, S. C.; Holm, R. H. *Inorg. Chem.* **1993**, *32*, 4745.

(46) The difluoro iron(III) derivative *trans*-Fe(Im)$_4$F$_2^+$BF$_4^-$ (Im = methylimidazole) has also been structurally characterized: Christie, S.; Subramanian, S.; Wang, L.; Zaworotko, M. J. *Inorg. Chem.* **1993**, *32*, 5415.

(47) (a) Rother, G.; Worzala, H.; Bentrup, U. *Z. Anorg. Allg. Chem.* **1996**, *622*, 1991. (b) Fourquet, J. L.; Plet, F.; Calage, Y.; de Pape, R. *J. Solid State Chem.* **1987**, *69*, 76. (c) Griebler, W.-D.; Babel, D. *Liebigs Ann. Chem.* **1980**, 1549. (d) For a comparison with bond distances observed in various structural types of Fe(III) fluorides, see: Leblanc, M.; Pannetier, J.; Ferey, G.; de Pape, R. *Rev. Chim. Min.* **1985**, *22*, 107.

Table 2. Selected Bond Lengths (Å) and Angles (deg) for Complexes $\mathbf{1^+PF_6^-}$, $\mathbf{2}$, $\mathbf{2^+PF_6^-}$, and $\mathbf{6^+BF_4^-}$

	1^+	2^a	2^+	6^+
Fe(l)−Cp(centroid)	1.766(4)	1.768(4)	1.780(9)	1.786(7)
Fe−X	1.856(2)	2.346(1)	2.237(2)	2.109(7)
Fe(1)−P(1)	2.3058(16)	2.197(1)	2.308(2)	2.275(2)
Fe(l)−P(2)	2.2899(14)	2.210(1)	2.276(2)	2.262(2)
Fe(l)−C(l)	2.146(4)	2.101(4)	2.133(9)	2.130(7)
Fe(1)−C(2)	2.131(4)	2.114(4)	2.160(9)	2.191(8)
Fe(1)−C(3)	2.125(4)	2.128(4)	2.147(8)	2.188(7)
Fe(1)−C(4)	2.150(4)	2.134(4)	2.148(9)	2.156(7)
Fe(1)−C(5)	2.148(4)	2.082(4)	2.134(9)	2.126(7)
P(1)−Fe(1)−P(2)	83.94(5)	84.98(5)	81.75(8)	84.77(7)
P(1)−Fe(1)−X	87.99(9)	86.03(4)	90.32(10)	91.76(17)
P(2)−Fe(1)−X	84.47(8)	87.23(5)	91.07(9)	83.56(17)
Cp(centroid)−Fe(1)−X	122.4(2)	120.0	119.9(3)	120.5(3)

^{a} From ref 19a.

between the covalent radii[48] of Cl and F (0.99−0.64 = 0.35 Å) suggest that the Fe−F covalent bond length should be around 1.89 Å, slightly longer than the experimental value of 1.856(2) Å obtained for complex $\mathbf{1^+PF_6^-}$. This difference between the observed and expected values indicates an increase in the Fe−F bond strength, suggesting that the *apparent* π contribution to the bonding is stronger in the fluoro than in the chloro compound. However, the Fe−F bond length is in agreement with that measured for octahedral Fe(III) porphyrinato complexes with Fe−F distances ranging from 1.792(3) to 1.966(2) Å,[45,46] and for the hexafluorometalate FeF_6^{3-} ions[47a−c] (Fe−F = 1.93 Å).

For the chloro complexes, X-ray crystal structures have now been determined for both the neutral[19a] and oxidized forms. The similarities in bond distances and angles in the two compounds (Table 2) suggest that the structural reorganization associated with the electron transfer is rather weak.[24,25e,44] Upon monoelectronic oxidation, a shortening (0.107 Å) of the Fe−Cl bond was observed with concomitant slight lengthening of the Fe−Cp* centroid and the Fe−P distances of 0.012 and ca. 0.09 Å, respectively. This is in accord with the computational findings, and consistent with a decrease of the $Fe(d_\pi)−Cl(p_\pi)$ electron repulsion (see below). A similar trend was also noted for the Cp*Fe(dppe) frameworks in the Fe(I/II) $Cp^*Fe(dppe)^{0/+}$ and Fe(II/III) $Cp^*Fe(dppe)(C\equiv C\text{-}1,4\text{-}C_6H_4NO_2)^{0/+}$ pairs, for which the crystal structures of both members of each couple have been determined.[25e,44] Oxidatively induced M−Cl bond shortenings were also seen for $Tp^*W(CO)Cl(MeCCMe)^{0/+}$ (0.09 Å),[36] $ReCl(CN^tBu)_3(PCy_3)_2^{0/+}$ (0.18 Å),[49] and $CpMoCl_2(PMe_3)_2^{0/+}$ (0.1 Å).[50]

The molecular structure of the methyl complex $\mathbf{6^+BF_4^-}$ is quite reminiscent of that of its methoxymethyl congener $Cp^*Fe(dppe)(CH_2OMe)^+PF_6^-$, with most bond lengths and angles falling into the same range.[43] The most remarkable structural difference is the shortening (0.106 Å) of the Fe−C(alkyl) bond, with a concomitant lengthening (0.016 Å) of the Fe−Cp* centroid distance when going from $\mathbf{6^+}$ to the methoxymethyl derivative. This lengthening/shortening interplay is presumably due to steric constraints imposed by the two bulky ancillary ligands when accommodating the alkyl group in the coordination sphere of the metal. In agreement with what has been observed for the Fe−Cl bond distances in $\mathbf{2^{0/+}}$ and with
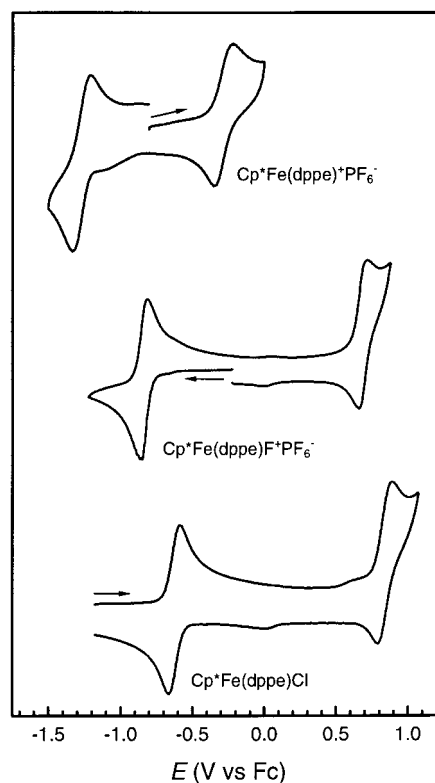
Figure 3. Cyclic voltammograms of $Cp^*Fe(dppe)^+PF_6^-$, $Cp^*Fe(dppe)F^+PF_6^-$, and $Cp^*Fe(dppe)Cl$ in THF/0.2 M $Bu_4N^+PF_6^-$ at $T = 25\ °C$ and a voltage sweep rate $\nu = 1.0$ V s^{-1} at a Pt disk electrode ($d = 0.4$ mm).

the computational findings (see below and Table 5), the Fe−C(alkyl) distances of these two 17-electron Fe(III) complexes are shorter than the Fe−C(alkyl) bond length (2.154(4) Å) measured for the neutral Fe(II) benzyl derivative CpFe(dppe)-(CH_2Ph).[51] This contrasts with the small elongation (0.016 Å) of the Fe−C(alkynyl) distance observed in the *p*-nitrophenylalkynyl derivative $Cp^*Fe(dppe)(C\equiv C\text{-}1,4\text{-}C_6H_4NO_2)$ upon one-electron oxidation.[44]

The synthesis and spectroscopic characterization of the other $Cp^*Fe(dppe)X^{n+}$ complexes discussed in this paper [X = Cl ($\mathbf{2/2^+}$), I ($\mathbf{4}$), H ($\mathbf{5/5^+}$), Me ($\mathbf{6/6^+}$)] as well as the crystal structures of $\mathbf{2}$ and $\mathbf{5^+PF_6^-}$ have been described previously.[19] As a result of the present preparative work, *both members of each of the six redox couples under investigation have been isolated in high yields and fully characterized by spectroscopic methods and, in part, by X-ray crystal structure determinations.*

II. Electrochemical Studies and Thermochemical Results. Cyclic Voltammetry Studies. The electrochemical investigation of the complexes was performed in THF/0.2 M $Bu_4N^+PF_6^-$. The solvent THF offers good solubility of all species that were investigated, and is rather inert (at least on the experimental time scale) toward even the most reactive of the species, including the $Cp^*Fe(dppe)^{\bullet/+}$ couple. Possible consequences of solvent effects and/or ion pairing with the supporting electrolyte will be addressed later.

Figure 3 shows cyclic voltammograms for $Cp^*Fe(dppe)^+PF_6^-$, $Cp^*Fe(dppe)F$, and $Cp^*Fe(dppe)Cl$ in THF/0.2 M $Bu_4N^+PF_6^-$ ($T = 20\ °C$, $\nu = 1.0$ V/s, $d = 0.4$ mm Pt disk electrode). As can be seen, the 16-electron cation $Cp^*Fe(dppe)^+$ is reversibly reduced to the 17-electron radical $Cp^*Fe(dppe)^\bullet$ and reversibly

(48) Pauling, L. *The Nature of the Chemical Bond*; Cornell University Press: New York, 1960.

(49) Heinekey, D. M.; Voges, M. H.; Barnhart, D. M. *J. Am. Chem. Soc.* **1996**, *118*, 10792.

(50) Krueger, S. T.; Poli, R.; Rheingold, A. L.; Staley, D. L. *Inorg. Chem.* **1989**, *28*, 4599.

(51) Hill, D. H.; Parvez, M. A.; Sen, A. *J. Am. Chem. Soc.* **1994**, *116*, 2889.

Table 3. Cyclic Voltammetry Data for the Oxidation of Cp*Fe(dppe) Derivatives[a]

compound FeX	E_1 (FeX/FeX$^+$)[b]	E_2 (FeX$^+$/FeX^{2+})[b]
Cp*Fe(dppe)[c]	−1.272	−0.290
Cp*Fe(dppe)H	−0.747	0.75[d]
Cp*Fe(dppe)CH$_3$	−0.883	0.56[d]
Cp*Fe(dppe)F[e]	−0.824	0.688
Cp*Fe(dppe)Cl	−0.618	0.823
Cp*Fe(dppe)Br	−0.582	0.811
Cp*Fe(dppe)I	−0.540	0.780

[a] THF/0.2 M Bu$_4$N$^+$PF$_6^-$, T = 20 °C, Pt disk electrode (d = 0.4 mm), voltage sweep rate v = 1.0 V/s. [b] Oxidation potential, V vs Cp$_2$Fe/Cp$_2$Fe$^+$. The voltammograms were reversible unless otherwise stated, and potentials are taken as the midpoints between anodic and cathodic peaks. Values are the average of 3 separate measurements and are reproducible to within ±5 mV. [c] Measurements were done on Cp*Fe(dppe)$^+$PF$_6^-$ which, contrary to Cp*Fe(dppe)$^•$, is stable in THF at room temperature. [d] Peak potential for the irreversible process. [e] Measurements were performed on Cp*Fe(dppe)F$^{•+}$PF$_6^-$.
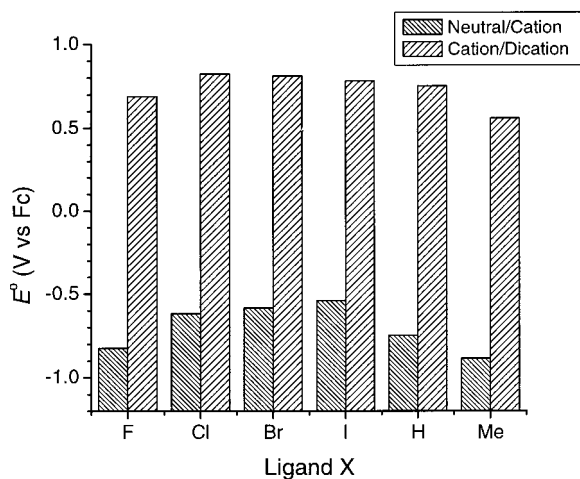
Figure 4. Electrode potential data for the Cp*Fe(dppe)X$^{0/+}$ and Cp*Fe(dppe)X$^{+/2+}$ couples (X = H, Me, F, Cl, Br, I) in THF/0.2 M Bu$_4$N$^+$PF$_6^-$.

oxidized to the 15-electron dication radical Cp*Fe(dppe)$^{2+}$, as described previously.[25e] The cyclic voltammograms of Cp*Fe-(dppe)F and Cp*Fe(dppe)Cl exhibit reversible oxidations to the 17-electron radical cations as well as to the 16-electron dications. It is immediately apparent from the figure that the fluoro complex is easier to oxidize than the chloro complex. Table 3 summarizes the electrode potential data obtained by cyclic voltammetry for the [Fe*]X$^{0/+}$ and [Fe*]X$^{+/2+}$ couples for X = H, CH$_3$, F, Cl, Br, and I. All neutral/monocation redox processes in Table 3 were chemically reversible, near-Nernstian processes (ΔE_p = 65−85 mV). Remarkably, except for X = H and CH$_3$, the cation/dication couples were also reversible. Steric and electronic protection of the metal center in the electron-rich, sterically demanding Cp*Fe(dppe) moiety must be important for the stabilization of the various oxidation states.

To the best of our knowledge, the electrochemical data for these halides constitute the first report of *reversible* oxidation potentials for a complete organometallic L$_n$M−X series (X = F, Cl, Br, I), regardless of the identity of the L$_n$M fragment. (After our initial communication,[26] other series have been reported with trends that fully agree with our results.[28b,36]) The reversible oxidation to monocation occurs most readily for the most electronegative halide and becomes progressively more difficult in the series F < Cl < Br < I, as visualized in Figure 4. This trend is the opposite of that predicted on the basis of halide electronegativities alone. The particularly large jump,

greater than 0.2 V, in the $E°$([Fe*]X$^{0/+}$) value for X = F relative to Cl and the other halides *apparently* supports the idea that F acts as an exceptionally good π donor. The fluoride stands out for the cation/dication oxidations too, although the overall halide trend is less clear-cut in this case. We will address the fluoride effect in more detail in the theoretical part of this paper (vide infra).

Consequences of Oxidation on the Homolytic [Fe*]−X Bond Energies. Equation 1 shows that an oxidatively induced M−X bond weakening will result if the L$_n$M−X compound is oxidized at more positive electrode potentials than the radical L$_n$M$^•$. This situation pertains to all compounds included in Table 3, i.e., an oxidatively induced bond weakening occurs in [Fe*]−X not only for X = H, but also for CH$_3$ as well as all halides. The bond energy changes, obtained from eq 1, are summarized in Table 4. Bond energy changes pertaining to the oxidation of Cp*Fe(dppe)X$^{•+}$ to the dications Cp*Fe(dppe)X^{2+} can be similarly estimated by replacing $E°_{ox}$(M$^•$) and $E°_{ox}$(MX) with $E°_{ox}$(M$^+$) and $E°_{ox}$(MX$^+$), respectively, in eq 1, and are also included in Table 4. Since all [Fe*]−X$^+$ are oxidized at more positive potentials than [Fe*]$^+$, the result of the second oxidation process is a further bond weakening for all X. Thus, the data demonstrate that for all X studied, [Fe*]−X bond energies decrease in the order [Fe*]X > [Fe*]X$^{•+}$ > [Fe*]X^{2+}. For both oxidation processes, there is a very interesting and obvious trend in the bond activation for the halides. The oxidatively induced bond weakening decreases in the order I > Br > Cl > F and is particularly less pronounced for F than for the other halides. In particular, the difference between F and the other halides is greater than 30 kJ/mol for the overall two-electron oxidation, which in principle corresponds to the generation of a vacant coordination site. This quantity may be viewed as an extra stabilization of the unsaturated 16-electron complex Cp*Fe-(dppe)X^{2+} that is provided by F, relative to the other halides. To the extent that this picture is valid and within the context of the involvement of halide p$_\pi$ to metal d$_\pi$ donation, which is quite easy to visualize (Figure 5), this phenomenon might be attributed to a more efficient π donation from F to the metal. The p$_\pi$−d$_\pi$ interaction may then be visualized as repulsive for an 18-electron metal center and relatively strongly bonding for a 16-electron metal center. An intermediate situation arises for a 17-electron center; this bonding picture is very similar to the simple bonding picture that has been used to describe the interaction between a 17-electron metal radical and a two-electron donor ligand to form 19-electron species.[52]

Consequences of Oxidation on the Heterolytic [Fe*]−X Bond Energies. Relative *heterolytic* bond dissociation energies (to be denoted BDE$_{het}$) between two oxidation states may be estimated from eq 2, which is derived from the thermochemical cycle in Scheme 3. The data obtained will be Gibbs free energy based since an assumption regarding canceling solvation contributions will not be valid when different charges apply to the two redox couples that are involved.

$$\Delta BDE_{het} = BDE_{het}(MX^{•+}) - BDE_{het}(MX) =$$
$$F[E°_{ox}(M^+) - E°_{ox}(MX)] \quad (2)$$

Equation 2 shows that an oxidatively induced heterolytic M−X bond strengthening will result if the L$_n$M−X compound is oxidized at more negative electrode potentials than the 16-

(52) (a) Therien, M. J.; Trogler, W. C. *J. Am. Chem. Soc.* **1988**, *110*, 4942. (b) Trogler, W. C. In *Metal−Ligand Interactions: From Atoms, to Clusters, to Surfaces*; Salahub, D. R., Russo, N., Eds.; Kluwer Academic Publishers: Dordrecht, The Netherlands, 1992; p 287. (c) Tyler, D. R. *Acc. Chem. Res.* **1991**, *24*, 325.

Table 4. Relative Homolytic and Heterolytic Bond Dissociation Energies for Cp*Fe(dppe)X^{n+} Complexes (kJ/mol)[a]

compound	$\Delta BDE_{hom}(MX^+-MX)$	$\Delta BDE_{hom}(MX^{2+}-MX^+)$	$\Delta BDE_{hom}(MX^{2+}-MX)$	$\Delta BDE_{het}(MX^+-MX)$
Cp*Fe(dppe)F (**1**)	−43	−4	−138	52
Cp*Fe(dppe)Cl (**2**)	−63	−107	−171	32
Cp*Fe(dppe)Br (**3**)	−67	−106	−173	28
Cp*Fe(dppe)I (**4**)	−71	−103	−174	24
Cp*Fe(dppe)H (**5**)	−51	−100[b]	−151[b]	44
Cp*Fe(dppe)CH$_3$ (**6**)	−38	−82[b]	−120[b]	57

[a] Obtained using the data in Table 3 and eqs 1 and 3. Note that negative values signify a bond weakening and positive values a bond strengthening upon oxidation. [b] Errors caused by unknown kinetic potential shift arising from irreversible electrode process are not taken into account.
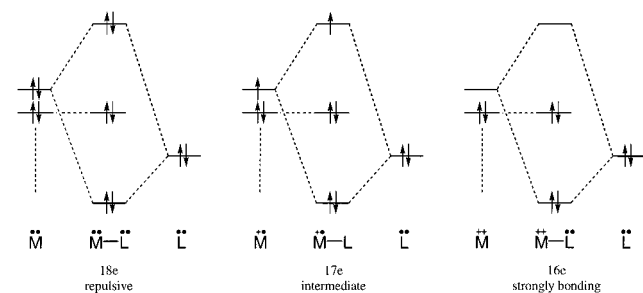
Figure 5. Simplified MO diagram depicting the consequences of M(d$_\pi$)−X(p$_\pi$) interactions in 18-, 17-, and 16-electron complexes.

Scheme 3
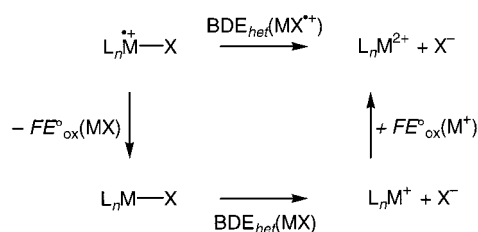
electron cation L$_n$M$^+$, which is in the same formal oxidation state but bears a formal positive charge. This situation pertains to all compounds included in Table 3. (The consequences of solvent and ion pairing effects, expected to be particularly strong for the MX$^{+/2+}$ couple, will be addressed later.) The ΔBDE_{het} data that are calculated from eq 2 are included in Table 4. The data show that all bonds are strengthened in the heterolytic sense as a consequence of the oxidation. It is not too surprising that a bond strengthening is observed—after all, the heterolytic cleavage of [Fe*]X involves the separation of singly charged cations and anions whereas the cleavage of [Fe*]X$^+$ involves the separation of a singly charged anion from a *doubly charged* cation. For the halide series, the bond strengthening decreases with increasing size of X in the order F > Cl > Br > I, in accord with important contributions from electrostatic effects.

Consequences of Solvent and Ion Pairing Effects. Poli et al. have rightfully pointed out that great care should be exerted when thermochemical cycles are used to estimate M−H BDE$_{hom}$ variations.[21] It was suggested that the 16-electron cation M$^+$ (and to a lesser and variable extent also the 17-electron species M$^•$ and MH$^{•+}$) is highly likely to establish strong interactions with the polar solvent or with the supporting electrolyte used for the electrochemical measurements. If this interaction with the medium is stronger for M$^+$ than for MH$^{•+}$, the result will be that M$^•$ is more readily oxidized compared to MH$^{•+}$ than what would be the case in the absence of interactions with the medium. The result would be a skewing of calculated BDE$_{hom}$ changes toward a bond weakening following oxidation.

To probe the possible involvement of solvent and ion pairing effects, we performed a thorough study in which solvent and supporting electrolyte counterions were varied. The following solvent (0.1 M supporting electrolyte) combinations were checked: MeCN (Bu$_4$N$^+$PF$_6^-$, Bu$_4$N$^+$BAr$_f^-$); THF (Bu$_4$N$^+$PF$_6^-$, Bu$_4$N$^+$BF$_4^-$, Bu$_4$N$^+$BAr$_f^-$); CH$_2$Cl$_2$ (Bu$_4$N$^+$PF$_6^-$, Bu$_4$N$^+$BAr$_f^-$); C$_6$H$_5$CF$_3$ (Bu$_4$N$^+$BF$_4^-$, Bu$_4$N$^+$BAr$_f^-$); and C$_6$H$_5$F (Bu$_4$N$^+$BF$_4^-$, Bu$_4$N$^+$BAr$_f^-$).[53] The Cp*Fe(dppe)H$^{0/+}$ and Cp*$_2$Fe$^{0/+}$ couples were investigated in all these combinations, whereas the Cp*Fe(dppe)$^{0/+}$ couple was checked in the THF, C$_6$H$_5$CF$_3$, and C$_6$H$_5$F media only due to the limited stability of Cp*Fe(dppe)$^+$ in MeCN and CH$_2$Cl$_2$. It was found that $E°$([Fe*]H$^{0/+}$) vs $E°$(Cp$_2$Fe$^{0/+}$) varied over a 0.18 V range in these media. However, $E°$([Fe*]H$^{0/+}$) varied over only a 0.04 V range when referenced against $E°$(Cp*$_2$Fe$^{0/+}$) in the same solvent/electrolyte systems, demonstrating that the variations for the iron hydride relative to Cp$_2$Fe are primarily due to medium effects on the Cp$_2$Fe$^{0/+}$ couple, rather than on the hydride complex. (Ruiz and Astruc[54] have recently advocated the use of Cp*$_2$Fe as an electrochemistry standard instead of Cp$_2$Fe because the former is much less subject to solvent and counterion effects.) Thus, no significant specific interactions between the solvent or counterion and the iron hydride redox couple appeared to complicate the electrode potential determinations. On the other hand, $E°$(Cp*Fe(dppe)$^{0/+}$) variations constituted less than 0.17 V, when referenced against Cp*$_2$Fe$^{0/+}$. These variations, in part caused by less than ideal CV response for this couple, are greater than those for Cp*Fe(dppe)H$^{0/+}$, but still small enough that we conclude that no *strong* specific interactions with the counteranion or solvent molecules exist for the Cp*Fe(dppe)$^{0/+}$ couple. Combining the data for Cp*Fe(dppe)H$^{0/+}$ and Cp*Fe(dppe)$^{0/+}$, the difference between their $E°$ values showed a 0.13 V variation (translating to ca. 13 kJ/mol difference in ΔBDE_{hom} data). We conclude that the electrode potentials are relatively uncomplicated by medium effects and that the oxidatively induced BDE$_{hom}$ weakening effects that are calculated for the 17-electron cations are undoubtedly real.

Ion pairing is, however, bound to influence the data for the dications much more strongly. For example, in THF/0.1 M Bu$_4$N$^+$BAr$_f^-$, the Cp*Fe(dppe)$^{+/2+}$ couple exhibited a very broad and chemically *irreversible* wave, contrasting the reversibility of the process in THF/0.1 M Bu$_4$N$^+$PF$_6^-$. Thus, the apparent stability of the 15-electron dication Cp*Fe(dppe)$^{2+}$ on the CV time scale appears to be due to electrostatic attraction and stabilization by the (relatively speaking) small counteranion PF$_6^-$. Ironically, it is the very same counterion that causes its demise in the fluoride abstraction reaction that gives **1**$^+$. There

(53) For the merits of using (C$_6$F$_5$)$_4$B$^-$ or BAr$_f^-$ as the anion in the supporting electrolyte, see: (a) Hill, M. G.; Lamanna, W. M.; Mann, K. R. *Inorg. Chem.* **1991**, *30*, 4687. (b) LeSuer, R. J.; Geiger, W. E. *Angew. Chem., Int. Ed.* **2000**, *39*, 248. For the use of C$_6$H$_5$CF$_3$ as a solvent for CV investigations of organometallic species, see: (c) Ohrenberg, C.; Geiger, W. E. *Inorg. Chem.* **2000**, *39*, 2948. Whereas C$_6$H$_5$F appears unexplored as a solvent for CV investigations of organometallics, its use has been recently described for the synthesis of unsaturated Ru complexes: (d) Tenorio, M. J.; Mereiter, K.; Puerta, M. C.; Valerga, P. *J. Am. Chem. Soc.* **2000**, *122*, 11230.

(54) Ruiz, J.; Astruc, D. *C. R. Acad. Sci., Ser. IIc: Chim.* **1998**, *1*, 21.

Table 5. Selected Optimized Metrical Data of the Models CpFe(dpe)X$^{0/+}$ (X = F, Cl, Br, I, H, CH$_3$) with Available X-ray Data of Related Cp*Fe(dppe)X$^{0/+}$ Complexes in Italics

compound [Fe] = CpFe(dpe)		Fe–X (Å)	Fe–P (Å)		Fe–C(Cp) (Å) av (range)	P–Fe–X (deg)		'Cp'–Fe–X^a (deg)
[Fe]F		1.927	2.18	2.17	2.11 (2.08–2.13)	90	86	124
[Fe]F$^+$		1.816	2.26	2.25	2.16 (2.13–2.20)	91	89	127
		1.856	*2.31*	*2.29*	*2.14 (2.13–2.15)*	*88*	*84*	*122*
[Fe]Cl		2.343	2.18	2.17	2.11 (2.09–2.13)	89	87	124
		2.346	*2.21*	*2.20*	*2.11 (2.08–2.13)*	*87*	*86*	*120*
[Fe]Cl$^+$		2.208	2.26	2.25	2.16 (2.14–2.19)	93	91	126
		2.239	*2.31*	*2.27*	*2.14 (2.12–2.16)*	*90*	*90*	*119*
[Fe]Br		2.503	2.19	2.18	2.11 (2.09–2.13)	89	87	124
[Fe]Br$^+$		2.370	2.26	2.25	2.16 (2.13–2.18)	93	91	126
[Fe]I		2.739	2.18	2.18	2.12 (2.09–2.13)	89	91	121
[Fe]I$^+$		2.584	2.26	2.25	2.16 (2.14–2.18)	92	95	126
[Fe]H^b	HA	1.515	2.15	2.15	2.12 (2.11–2.14)	87	86	121
	HB	1.519	2.15	2.15	2.13 (2.11–2.15)	82	81	120
[Fe]H$^{+\,b}$	HB$^+$	1.513	2.23	2.22	2.14 (2.12–2.16)	75	75	112
	HC$^+$	1.510	2.25	2.20	2.16 (2.12–2.21)	100	75	121
		1.55	*2.21*	*2.20*	*2.11 (2.08–2.15)*	*77*	*69*	*120*
[Fe]CH$_3$		2.075	2.16	2.15	2.13 (2.12–2.14)	91	90	122
[Fe]CH$_3^+$		2.022	2.25	2.24	2.18 (2.12–2.25)	93	92	125
		2.105	*2.27*	*2.26*	*2.16 (2.12–2.20)*	*91*	*84*	*121*

^{a} 'Cp' = C$_5$H$_5$ centroid. ^{b} HA and HB, and HA$^+$ and HC$^+$ are the DFT-optimized geometries obtained for CpFe(dpe)H and CpFe(dpe)H$^+$, respectively (see text).

may also be significant ion-pairing interactions that influence the electrode potential data for the [Fe*]X$^{+/2+}$ electrode processes. This will affect the ΔBDE data involving the dications, as well as the heterolytic BDE data for the monocations, but *not* the ΔBDE data that involve the monocation vs neutral complexes.

Calculational Studies

The electrochemical experiments described above allowed the experimental determination of relative BDE values. A better insight into the factors influencing the variation of these relative BDE values within the studied series of compounds can be obtained by determination of absolute BDE values. Moreover, the knowledge of absolute BDE values allows a more complete bonding analysis of each individual complex. This can be done theoretically at a reasonable level of accuracy. This is why we have carried out density functional (DFT) calculations on model complexes of the [Fe*]X$^{0/+}$ series. Because of complications arising from large solvent/electrolyte effects in solution (which cannot be modeled) and from their open-shell configuration, the 16-electron [Fe*]X^{2+} complexes were not investigated theoretically. Details of the calculations are given in the Experimental Section.

Optimized Geometries. All the optimized geometries of the models CpFe(dpe)X$^{0/+}$ (X = F, Cl, Br, I, CH$_3$) are very close to the C_s symmetry and adopt the pseudooctahedral three-legged piano-stool structure. The somewhat peculiar case of X = H will be discussed later. Selected metrical parameters for the models CpFe(dpe)X$^{0/+}$ (X = F, Cl, Br, I, H, CH$_3$) optimized by DFT calculations are given in Table 5, together with available X-ray experimental data of their Cp*Fe(dppe)X$^{0/+}$ relatives for comparison. A good agreement is obtained between the optimized geometries and the X-ray molecular structures. The optimized Fe–C and Fe–P distances tend to be slightly shorter than the experimental ones. It has been shown in previous calculations[55] that this shortening (about 0.01 and 0.05 Å for Fe–C and Fe–P, respectively) is a consequence of the replacement of Cp* by Cp and dppe by dpe in the models. The Fe–X bond lengths are also in good agreement with the available experimental data (deviation 0.01–0.04 Å) in the cases of X =
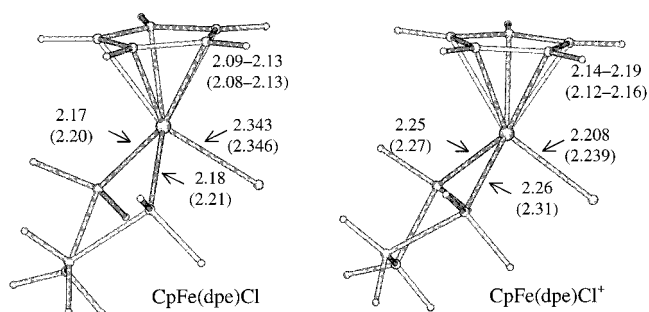
(55) Costuas, K.; Saillard, J.-Y. *Organometallics* **1999**, *18*, 2505.

Figure 6. Optimized geometries of CpFe(dpe)Cl$^{0/+}$ (distances are given in Å). The X-ray distances of Cp*Fe(dppe)Cl$^{0/+}$ are given in parentheses.

H, F, Cl. A larger deviation is found for X = CH$_3$ (0.08 Å). The P–Fe–X and Cp(centroid)–Fe–X angles differ only by 1–8°, values barely significant at our level of theory and modeling. In the series of the neutral 18-electron species, the average Fe–P and Fe–C separations are roughly constant within the halogen series. They increase in the order H ∼ CH$_3$ < halogens. This order is somewhat different for the series of the 17-electron cations for which the average Fe–P order is H < CH$_3$ ∼ halogens and the average Fe–C order is H < F ∼ Cl < Br ∼ I ∼ CH$_3$. The oxidation of CpFe(dpe)X leads to Fe–P and Fe–C bond lengthening, by 0.07–0.09 and 0.03–0.05 Å, respectively. On the other hand, the Fe–X bond distances are somewhat shortened, by approximately 0.2% (X = H), 3% (X = CH$_3$), and 5–6% (X = halogens). Therefore, the oxidation of the neutral species has the same structural effect on all the complexes. The X-ray structures of both the neutral and monocationic species are known in the case of X = Cl as discussed earlier, and provide a good test for probing the agreement between theory and experiment (see Table 5 and Figure 6).

We discuss now the X = H case in more detail. Unlike for the X ≠ H species, geometry optimization of CpFe(dpe)H lead to two minima (see Figure 7), both of them characterized by frequency calculations. One of them, denoted HA, has a symmetry close to C_s and adopts a three-legged piano-stool conformation comparable to those obtained for the X ≠ H species. In the other one, named HB, the P–Fe–P plane is much
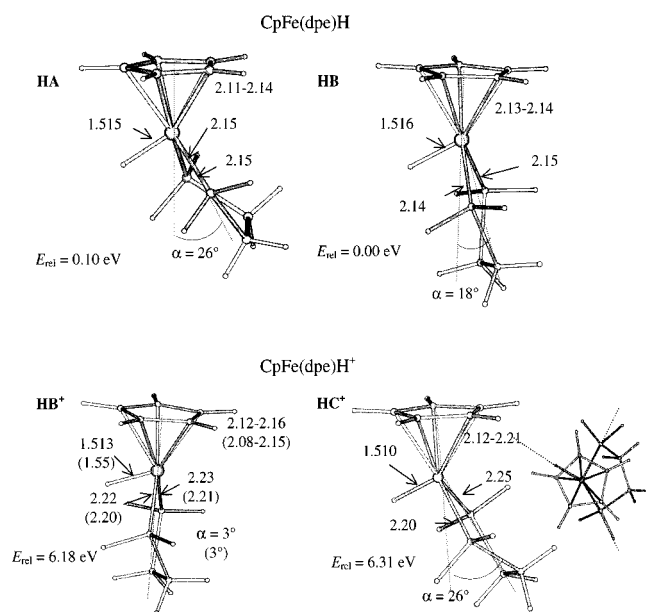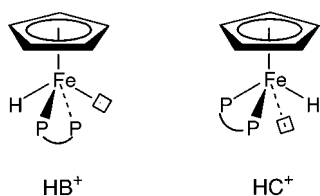
Figure 7. Optimized geometries of CpFe(dpe)H$^{0/+}$ (distances are given in Å). The X-ray distances of Cp*Fe(dppe)D$^+$ are given in parentheses. E_{rel} = computed relative energy.

Scheme 4

closer to being perpendicular to the Cp plane (Figure 7). HB is more stable than HA by 0.10 eV. The exploration of the potential energy surface around HA and HB indicated that this surface is rather flat. The search for other minima for CpFe(dpe)H was unsuccessful. Since the X-ray structure of Cp*Fe(dppe)H is not available so far, there are no experimental data to support the theoretical results for this neutral species.

Two minima, characterized by frequency calculations, were also found for CpFe(dpe)H$^+$ (Figure 7). The more stable by 0.13 eV (HB$^+$) has a geometry related to that of HB in which the P−Fe−P and Cp planes are almost perfectly perpendicular. The other isomer (HC$^+$) has a very unsymmetrical structure that is different from both HA and HB. One can idealize the geometries of HB$^+$ and HC$^+$ by considering that they are the two possible positional isomers of a four-legged piano-stool CpFe(dpe)H$^+$ complex in which one leg is occupied by a vacant site, as sketched in Scheme 4. These types of distortions away from the pseudooctahedral three-legged piano-stool have been recently described by Poli and co-workers in the case of 16-electron molybdenum complexes.[56] It turns out that the X-ray structure[19b] of Cp*Fe(dppe)D$^+$ is close to HB$^+$ (Figure 7). The agreement between the experimental and calculated bond angles is particularly good (see also Table 5).

Ionization Potentials. The first diabatic ionization potentials of the CpFe(dpe)X models are reported in Table 6, together with the energies and localization of the LUMO and of the three highest occupied MO's of these 18-electron complexes. For the pseudooctahedral three-legged piano-stool complexes, these

three orbitals are usually referred to as the "t$_{2g}$" set.[57] They have a dominant Fe character and are nonbonding with respect to the σ-type interactions. Their major character is sketched in Scheme 5. The particular case of X = H will be discussed in more detail later. Analysis of the electronic structure of the 17-electron cationic species indicates that the oxidation always involves the HOMO.

The computed ionization potentials follow the order I ∼ Br > Cl > H > F > CH$_3$. They are consistent with the energy order of the HOMO's. It has been shown that DFT-computed ionization potentials within a homogeneous series of transition-metal complexes correlate linearly with the corresponding experimental redox potentials.[58] Figure 8 shows the calculated first ionization potentials (in eV) of the CpFe(dpe)X complexes plotted against the first oxidation potentials of the Cp*Fe(dppe)X series (in mV). A nice linear correlation is obtained for the X ≠ H series (least-squares correlation factor = 0.99; slope = 0.96), providing confidence in the consistency of the theoretical and electrochemical approaches.

In the case of X = H, two squares are found in the diagram. They correspond to the oxidation of the HA and HB conformers, the oxidized species being HB$^+$ in both cases. When the considered oxidized species is HC$^+$, the computed ionization potentials of HA and HB are 6.31 and 6.40 eV, respectively, i.e., farther from the least-squares curve. It is noteworthy that the ionization potential of the computed less stable conformer HA lies closer to the correlation line than the more stable HB conformer. Obviously, the hydride species behave differently compared to the other members of the studied series.

Bond Dissociation Energies. The computed homolytic (BDE$_{hom}$) and heterolytic (BDE$_{het}$) Fe−X bond energies of the [Fe]X$^{0/+}$ models are given in Tables 7 and 8, respectively. Values calculated with and without BSSE corrections are reported. The effect of the BSSE corrections does not change the BDE order within the series, except for X = H.

In the case of a homolytic dissociation, the BDE$_{hom}$ order is computed as F > Cl > Br > H > I > CH$_3$, for both the neutral and the cationic series. In agreement with the electrochemical data, all the BDE$_{hom}$ values of the 17-electron species are lower than those of their 18-electron parents. However, the theoretical Δ(BDE$_{hom}$) values differ significantly from the experimental ones. This difference probably originates mainly from the fact that the former correspond to isolated molecules, while the latter refer to molecules in solution. It is likely that interactions with the solvent and electrolyte molecules constitute the major effect responsible for this discrepancy between theory and experiment. Nevertheless, there is a nice linear correlation between both series of data, as exemplified by the plot in Figure 9a (least-squares correlation factor = 0.99; slope = 0.71). The least-squares fit does not include the X = H case which, like in Figure 8, makes an exception. Being significantly different from 1, the slope of the curve depends also on solvation energies which cannot be considered as being constant within the series. The Y-intercept of the least-squares curve is −15.7 kJ/mol. This value corresponds to all the intermolecular energy terms which are not considered in the calculations and which can be considered constant within the series. Deviations in absolute numbers will also arise from the fact that comparisons are made between experimentally derived enthalpy data in solution at room

(56) Cacelli, I.; Poli, R.; Quadrelli, E. A.; Rizzo, A.; Smith, K. M. *Inorg. Chem.* **2000**, *39*, 517.

(57) Albright, T. A.; Burdett, J. K.; Wangbo, M.-H. *Orbital Interactions in Chemistry*; John Wiley: New York, 1985.

(58) (a) Bruce, M. I.; Low, P. J.; Costuas, K.; Halet, J.-F.; Best, S. P.; Heath, G. A. *J. Am. Chem. Soc.* **2000**, *122*, 1949. (b) Ogliaro, F.; Halet, J.-F.; Astruc, D.; Saillard, J.-F. *New J. Chem.* **2000**, *24*, 257.

Table 6. Energy and Localization of the Frontier Orbitals and Diabatic First Ionization Potential (IP) of CpFe(dpe)X (X = H, CH₃, F, Cl, Br, I)

compound [Fe] = CpFe(dpe)		[Fe]F	[Fe]Cl	[Fe]Br	[Fe]I	[Fe]H[a] HA/HB	[Fe]CH₃
HOMO-2	% Fe − % X	73−6	69−12	69−14	67−14	84−0/85−0	81−2
	E (eV)	−4.96	−5.05	−5.05	−5.09	−4.89/−4.84	−4.75
HOMO-1	% Fe − % X	72−19	67−25	65−29	46−49	73−1/85−0	77−3
	E (eV)	−4.43	−4.67	−4.72	−4.77	−4.29/−4.20	−4.33
HOMO	% Fe − % X	67−17	64−22	63−24	55−53	83−0/74−1	82−3
	E (eV)	−4.00	−4.25	−4.32	−4.39	−4.21/−4.17	−3.97
LUMO	% Fe − % X	60−11	57−15	57−16	54−18	60−0/50−0	55−0
	E (eV)	−2.14	−2.42	−2.52	−2.68	−1.77/−1.74	−1.83
IP[b] (eV)		6.11	6.31	6.38	6.37	6.18/6.27	6.06

[a] The two sets of values correspond to the 2 DFT optimized structures of CpFe(dpe)H, HA, and HB (see Figure 7 for label). [b] IP calculated considering HB⁺ as the oxidized species.

Scheme 5
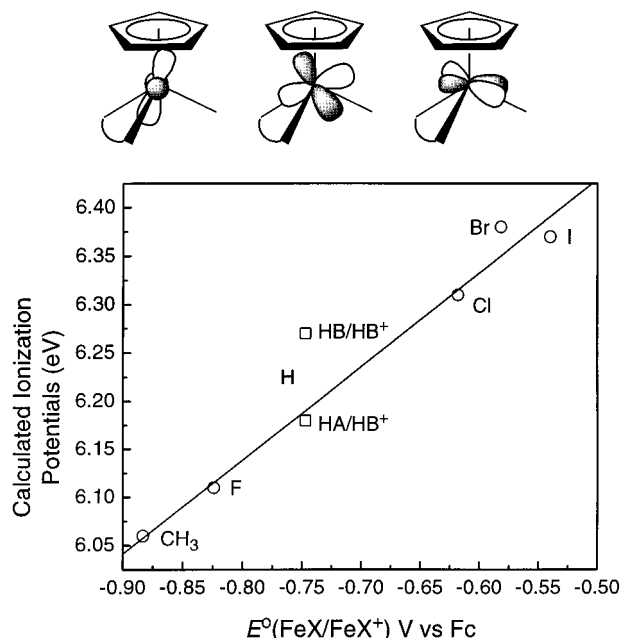
Figure 8. Calculated ionization potentials of [Fe]X models plotted against the first oxidation potentials of the [Fe*]X series, X = H, CH₃, F, Cl, Br, I. For X = H, the square spots correspond to the ionization potentials of HA and HB, the oxidized species being HB⁺ (cf. Figure 7).

temperature and theoretically derived energy data for a single molecule at 0 K.

In the case of a heterolytic dissociation, the BDE$_{het}$ order is computed as H > CH₃ > F > Cl > Br > I, for both the neutral and the cationic series. In agreement with the electrochemical data, the BDE$_{het}$ values of the 17-electron species are all greater than those of their 18-electron parents. The theoretical ΔBDE$_{het}$ values differ from the experimental ones to a larger extent than in the case of a homolytic dissociation. This is not surprising, owing to the larger solvent/electrolyte effect expected from the more ionic species involved in the heterolytic cycle. Nevertheless, there is a nice linear correlation between the experimental and calculated values, as shown in Figure 9b (least-squares correlation factor = 0.99; slope = 0.94). Again, the X = H case is not included in the least-squares fit. The Y-intercept of the least-squares curve is −386.9 kJ/mol. This value is much larger than that corresponding to the homolytic dissociation and is indicative of strong intermolecular interactions.

Analysis of the Theoretical Data. We begin the discussion by analyzing the X = H case, which provides a good reference starting point to understand the Fe−X π-type effects which are present in the other complexes, since the Fe−H interaction is of pure σ-type. Moreover, unlike when X ≠ H, two conformers were found for [Fe]H (HA and HB) and for [Fe]H⁺ (HB⁺ and HC⁺). HA adopts the three-legged piano-stool geometry, while HB⁰/⁺ and HC⁺ are related to the four-legged piano-stool conformation (see Figure 7 and Scheme 4). These latter conformations can be described as resulting from distortions away from the pseudooctahedral three-legged piano-stool geometry. Such distortions appear not to be allowed when X is a π donor. It is noteworthy that the optimization of the [Fe]H²⁺ dication in its singlet state led to a geometry of type HC²⁺ that was more stable than HB²⁺ by 0.21 eV. In this case, the ligand vacancy of Scheme 4 is a real coordination site. Owing to the rather small computed energy differences between the different conformers of [Fe]H and [Fe]H⁺, and on the differences between the [Fe] model and the [Fe*] "real" systems, it is difficult to make firm predictions on which of the conformations of [Fe*]H and [Fe*]H⁺ is predominant in solution during the electrochemical experiments. From the curves of Figures 8 and 9, one may tentatively suggest that the electroactive species correspond to conformations HA and HB⁺.

The shortest Fe−P bond distances in the neutral [Fe]X series correspond to X = H. This is somewhat counterintuitive since the σ and π covalent bonding interactions between Fe and the other ligands are expected to be weaker when competing with the strong σ-donor and non-π-donor hydride ligand, as compared to the weak σ-donor and π-donor fluoride ligand, for example. However, it has been shown recently that there is not always a strong correlation between the π-donor ability of a ligand and the distances between the metal and the other ligand.[59] As a matter of fact, the Fe−C(Cp) distances do not vary very much in the [Fe]X series.

The one-electron oxidation of [Fe]H corresponds to the partial depopulation of the highest component of the "t$_{2g}$" block (see above). One has to keep in mind that the metal−ligand π-type interactions of complexes such as CpFe(dpe)X will affect primarily the "t$_{2g}$" orbitals,[57] i.e. the metallic MO involved in the oxidation process has mixed in a bonding way with the π-accepting frontier orbitals of the phosphine and the cyclopentadienyl ligands. Therefore, the oxidation of CpFe(dpe)H corresponds to a loss of Fe−P and Fe−C π bonding, the consequence of which is bond elongation (see Table 5). On the other hand, there is no simple orbital argument to explain the slight shortening (if considered significant) of the Fe−H bond when going from CpFe(dpe)H to CpFe(dpe)H⁺. It may be attributed to some contraction of the metal atomic radius when going from Fe(II) to Fe(III). Such an ionic radius effect has

(59) Heyn, R. R.; MacGregor, S. A.; Nadasdi, T. T.; Ogasawara, M.; Eisenstein, O.; Caulton, K. G. *Inorg. Chim. Acta* **1997**, *259*, 5.

Table 7. Calculated Homolytic [Fe]−X BDE$_{hom}$ for the CpFe(dpe)X$^{0/+}$ Series[a]

		[Fe]F	[Fe]Cl	[Fe]Br	[Fe]I	[Fe]H HA/HB$^+$	[Fe]H HA/HC$^+$	[Fe]H HB/HB$^+$	[Fe]H HB/HC$^+$	[Fe]CH$_3$
BDE$_{hom}$ (MX) (eV)	without BSSE	4.58	3.48	3.15	2.67	2.95	2.95	3.04	3.04	2.00
	with BSSE	3.81	3.15	2.90	2.49	1.98	1.98	2.05	2.05	1.22
BDE$_{hom}$ (MX$^+$) (eV)	without BSSE	4.38	3.08	2.70	2.21	2.68	2.57	2.68	2.57	1.85
	with BSSE	3.65	2.87	2.56	2.15	1.72	1.61	1.72	1.61	1.12
ΔBDE$_{hom}$ (MX$^+$/MX) (kJ/mol)	with BSSE	−15.4	−27.7	−32.8	−32.8	−24.5	−35.7	−31.8	−42.4	−9.6

[a] ΔBDE$_{hom}$ = BDE$_{hom}$(MX$^+$) − BDE$_{hom}$(MX). Negative values indicate a bond weakening.

Table 8. Calculated Heterolytic [Fe]−X BDE$_{het}$ for the CpFe(dpe)X$^{0/+}$ Series[a]

		[Fe]F	[Fe]Cl	[Fe]Br	[Fe]I	[Fe]H HA/HB$^+$	[Fe]H HA/HC$^+$	[Fe]H HB/HB$^+$	[Fe]H HB/HC$^+$	[Fe]CH$_3$
BDE$_{het}$ (MX) (eV)	without BSSE	6.78	5.70	5.48	5.15	8.15	8.15	8.06	8.06	7.96
	with BSSE	6.65	5.78	5.58	5.30	7.90	7.90	7.99	7.99	7.74
BDE$_{het}$ (MX$^+$) (eV)	without BSSE	11.96	10.68	10.40	10.08	13.15	13.04	13.15	13.04	13.19
	with BSSE	11.16	10.11	9.85	9.57	12.45	12.39	12.45	12.39	12.33
ΔBDE$_{het}$ (MX$^+$/MX) (kJ/mol)	with BSSE	434.9	417.0	411.9	411.2	441.1	452.2	430.5	441.6	442.4

[a] ΔBDE$_{het}$ = BDE$_{het}$(MX$^+$) − BDE$_{het}$(MX). Positive values indicate a bond strengthening.
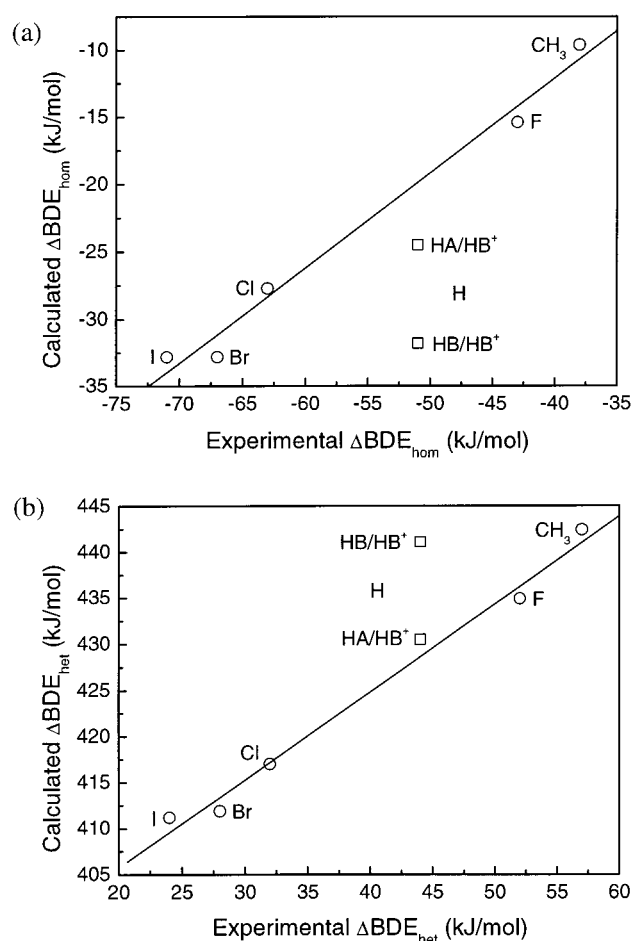

Figure 9. Calculated ΔBDE ([Fe]X/[Fe]X$^+$) plotted against the experimental ΔBDE ([Fe*]X/[Fe*]X$^+$), X = H, CH$_3$, F, Cl, Br, I: (a) homolytic dissociation and (b) heterolytic dissociation. For X = H, the square spots correspond to ΔBDE(HA/HB$^+$) and ΔBDE(HB/HB$^+$) (cf. Figure 7).

already been noticed in other systems.[50,60] The change appears not to be associated with a bond strengthening, since oxidation *lowers* the BDE (Table 7). Another result that is counterintuitive when confronted to the Fe−H BDE values is the increase in

the ν_{Fe-H} stretching frequency upon oxidation. The values computed for HA, HB, HB$^+$, and HC$^+$ are 1892, 1876, 1907, and 1921 cm^{-1}, respectively. These values agree well with the experimental data recorded at ambient temperature in Nujol mulls, 1869 and 1886 cm^{-1} for [Fe*]H and [Fe*]H$^+$, respectively.

Similarly to X = H, when X = CH$_3$ or halogen, the π-accepting properties of the phosphine and cyclopentadienyl ligands induce a lengthening of the Fe−P and Fe−C bonds upon oxidation of CpFe(dpe)X. However, the Fe−X bond is shortened to a much larger extent than in the X = H case, especially when X = halogen. Unlike hydrogen, these ligands have π-donor properties which cause the "t$_{2g}$" set to mix in an antibonding way with their low-lying π-type frontier orbitals (Figure 5). The removal of one electron from this set lowers the Fe−X π-type antibonding character, and is consequently expected to contribute to the shortening of this bond. Surprisingly, as for X = H, this shortening is associated with a *lowering* of the corresponding BDE (Table 7). The ν_{Fe-X} stretching frequency was computed in the case of X = Cl, for both the neutral and cationic complexes. As in the X = H case, an *increase* in the ν_{Fe-X} stretching frequency upon oxidation is found (from 279 cm^{-1} to 307 cm^{-1}), as was also observed experimentally (vide supra).

The ionization energies of the [Fe]X series (and the oxidation potentials of the [Fe*]X series) are ordered consistently according to their HOMO energies, with the highest HOMO corresponding to X = F and the lowest one corresponding to X = I (see Tables 3 and 6). Thus, within the halogen derivatives, it becomes increasingly difficult to oxidize [Fe]X when X changes from the top through the halogen column of the periodic table. As said above, this trend is unexpected from the point of view of the HSAB concept,[33] which predicts that the halide π-donor ability decreases in the series I > Br > Cl > F. In other words, the heavier X is, the closer in energy are the M(d$_\pi$) and X(p$_\pi$) orbitals in Figure 5, and consequently the stronger is their expected interaction and the higher is the antibonding HOMO. In favoring a larger overlap, the more diffuse valence AOs of the heavier halogens should favor the same trend, at least in the case of F, Cl, and Br. The so-called inverse halide order observed in the title complexes and reproduced in the calculations has already been noted in the literature.[28b,36,50,61]

(60) (a) Fettinger, J. C.; Kraatz, H.-B.; Poli, R.; Quadrelli, E. A. *J. Chem. Soc., Dalton Trans.* **1999**, 497. (b) See ref 21 and references therein.

(61) (a) Zietlow, T. C.; Hopkins, M. D.; Gray, H. B. *J. Am. Chem. Soc.* **1986**, *108*, 8266. (b) Hascall, T.; Rabinovich, D.; Murphy, V. J.; Beachy, M. D.; Friesner, R. A.; Parkin, G. *J. Am. Chem. Soc.* **1999**, *121*, 11402. (c) Krueger, S. T.; Owens, B. E.; Poli, R. *Inorg. Chem.* **1990**, *29*, 2001.

Table 6 shows that HOMO energy is *not* related to the π-donor ability of X. Indeed, it is clear that the amount of mixing of the X orbitals into the "t_{2g}" set follows the I > Br > Cl > F order, in perfect agreement with the expected π-donor order. This apparent contradiction between the HOMO energies and their X character can be explained by considering the ionic character of the Fe−X bond. In the case of fluorine, this small and electronegative atom acts effectively as a negative point charge located close to the metal, and this tends to destabilize the "t_{2g}" electrons, as has been previously suggested in an analysis of bonding in Vaska-type complexes.[9] When going down the halogen column, the Fe−X bond becomes less polar and longer. Both factors contribute to weaken the point charge effect, consequently leading to a lower lying HOMO.

The analysis of the Fe−X BDE variation across the CpFe(dpe)X$^{0/+}$ series might have been easy if it was possible to evaluate separately all its components (σ and π covalent, ionic, fragment relaxation components, ...). Unfortunately, this is not at all straightforward, especially in the case of the calculated compounds, owing to their low symmetry. With the ADF code it is, however, possible to carry out a partial decomposition of the computed BDE values by using the transition-state approach developed by Ziegler.[62] Since the fragmentation is made on the [Fe]X$^{0/+}$ molecules in their optimized geometries, this decomposition is carried out on bond dissociation energies which do not take into account the geometrical relaxation energy of the [Fe]$^{0/+/2+}$ fragments. In addition, they are computed within the spin-restricted formalism and they are not corrected from BSSE. These "unrelaxed" values are written as BDE*'s in the following. They differ somewhat from the BDE values but they exhibit similar major trends within the halogen series and between neutral and cationic species. In Ziegler's transition-state method,[62] BDE* values are decomposed into three terms. One of them, E_{elect}, corresponds to the electrostatic interaction between the unperturbed fragments. It is calculated from the electron densities of the isolated fragments under consideration. It contains attractive contributions associated with the interaction between the electron density of one fragment and the nuclei of the other fragment and a repulsive contribution associated with the interaction between the fragment electron densities. The Pauli repulsion term, E_{Pauli}, is also calculated from the densities of the unrelaxed fragment. It can be roughly approximated to the sum of what is called 4-electron/2-orbital repulsions in approximate MO theory.[63] Similarly, the orbital interaction energy term, E_{orb}, can be roughly approximated to the so-called 2-electron/2-orbital attractive interaction. Since the qualitative meaning of E_{Pauli} and E_{orb} is only approximate, we will discuss only the sum of these two terms which can be considered as being the covalent component of the interaction between the fragments, that is: BDE* $= -(E_{elect} + E_{Pauli} + E_{orb}) = -(E_{elect} + E_{Pauli+orb})$. The values of BDE*, E_{elect} and $E_{Pauli+orb}$, computed for the homolytic and heterolytic dissociations of the [Fe]X$^{0/+}$ series are listed in Tables 9 and 10, respectively.

Let us first analyze the more simple case, namely the heterolytic BDE* values (BDE$_{het}$*). All the $E_{Pauli+orb}$ terms are destabilizing, indicating that the unique 2-electron/2-orbital interaction arising from the building of the Fe−X bond is not large enough to counterbalance the strong 4-electron/2-orbital

(62) Ziegler, T. In *Metal−Ligand Interactions: From Atoms, to Clusters, to Surfaces*; Salahub, D. R., Russo, N., Eds.; Kluwer: Dordrecht, The Netherlands, 1992; p 367.
(63) (a) Landrum, G. A.; Goldberg, N.; Hoffmann, R. *J. Chem. Soc., Dalton Trans.* **1997**, 3605. (b) Rosa, A.; Baerends, E. J. *New J. Chem.* **1991**, *15*, 815.

Table 9. Energy Decomposition of Fe−X BDE$_{hom}$* for the CpFe(dpe)X$^{0/+}$ (X = H, CH$_3$, F, Cl, Br, I) Series

compound	$E_{orb+Pauli}$	E_{elect}	$-BDE_{hom}$*
[Fe]F	−3.073	−2.452	−5.525
[Fe]Cl	−1.351	−2.861	−4.212
[Fe]Br	−0.863	−2.931	−3.794
[Fe]I	−0.610	−2.225	−3.337
[Fe]H (HA)	−1.655	−2.693	−4.348
[Fe]CH$_3$	−0.118	−3.407	−3.526
[Fe]F$^+$	−3.823	−1.291	−5.114
[Fe]Cl$^+$	−1.966	−1.613	−3.579
[Fe]Br$^+$	−1.549	−1.559	−3.107
[Fe]I$^+$	−1.099	−1.545	−2.644
[Fe]H$^+$ (HB$^+$)	−1.606	−2.205	−3.813
[Fe]CH$_3$$^+$	−0.845	−2.355	−3.200

Table 10. Energy Decomposition of Fe−X BDE$_{het}$* for the CpFe(dpe)X$^{0/+}$ (X = H, CH$_3$, F, Cl, Br, I) Series

compound	$E_{orb+Pauli}$	E_{elect}	$-BDE_{het}$*
[Fe]F	+0.491	−7.457	−6.967
[Fe]Cl	+0.938	−6.811	−5.873
[Fe]Br	+1.032	−6.677	−5.646
[Fe]I	+0.828	−6.156	−5.328
[FeH] (HA)	+4.448	−12.803	−8.355
[Fe]CH$_3$	+3.656	−12.124	−8.236
[Fe]F$^+$	+0.800	−12.943	−12.142
[Fe]Cl$^+$	+0.767	−11.636	−10.870
[Fe]Br$^+$	+0.552	−11.146	−10.594
[Fe]I$^+$	+0.193	−10.491	−10.298
[Fe]H$^+$ (HB$^+$)	+5.452	−19.034	−13.583
[Fe]CH$_3$$^+$	+3.162	−16.684	−13.521

repulsions between the fragments. However, BDE* is dominated by E_{elect}, which is largely stabilizing due to fragment charges ([Fe]$^{+/2+}$ and X$^-$). Because of the larger cationic charge in the case of the [Fe]X$^+$ series, E_{elect} is more stabilizing. It follows that for a given X ligand, BDE$_{het}$* is larger in the cationic than in the neutral species. In the [Fe]X (X = halogen) series, the E_{elect} stabilization decreases with the size of X in the order F > Cl > Br > I. This can be interpreted as resulting from the fact that the smaller X is, the more punctual and close to the cation is its electron density. It follows that when going from [Fe]X to [Fe]X$^+$, the variation of E_{elect} (ΔE_{elect}), and by inference of ΔBDE_{het}*, decreases in the order F > Cl > Br > I.

Looking now at the homolytic BDE* values (BDE$_{hom}$*), one can notice that the $E_{Pauli+orb}$ terms are now stabilizing. This can be explained by the fact that the 2-electron/2-orbital interaction associated with the building of the Fe−X bond is now more important since one of the electrons involved originates from a high-lying metallic hybrid, as depicted schematically in Figure 10 (compare the top parts of Figures 10a,c and 10b,d). Although weaker than in the heterolytic process, the stabilizing E_{elect} terms still dominate the BDE$_{hom}$* values. Contrary to the heterolytic case, the E_{elect} stabilization is weaker in the cationic series. Indeed, the oxidation of the [Fe] fragment corresponds to the removal of a "t_{2g}" electron, i.e., an electron that is close to the X nucleus, inducing a loss of stabilizing contribution in E_{elect}. It follows that for a given X ligand, BDE$_{hom}$* is lower in the cationic than in the neutral species, despite the diminution of the Fe−X π-type repulsion upon oxidation (see Figure 10). Unlike the situation in the heterolytic case, the variation of E_{elect} when going from the neutral to the cationic species increases with the size of X within the halogen series. This can be explained by the fact that the mostly metal-centered electron that is involved in the oxidation process is more effectively screened by the halogen electron cloud when X is smaller.

homolytic dissociation

a)

b)

heterolytic dissociation

c)

d)
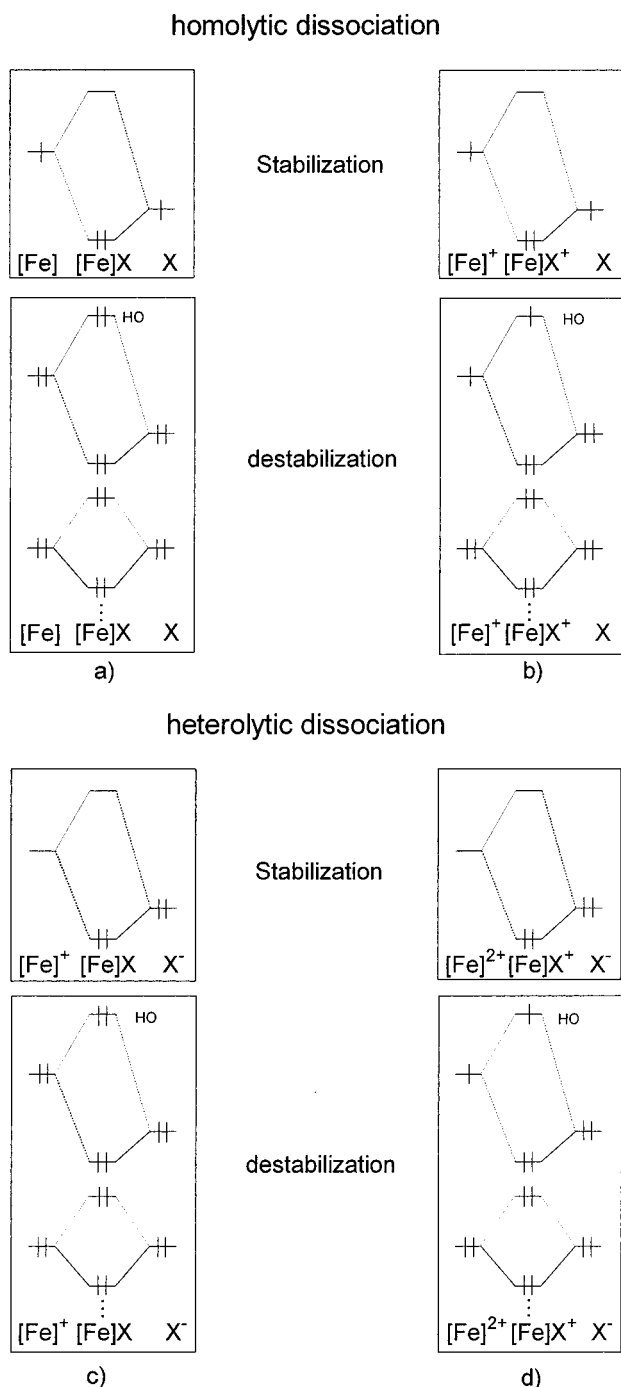
Figure 10. Major orbital interactions involved in the [Fe]X and [Fe]-X⁺ homolytic and heterolytic BDE values.

Concluding Remarks

Multiple methods of investigation have established that in the halide series, the electron density at the metal decreases in the series F > Cl > Br > I. This is corroborated experimentally through the oxidation potentials for the [Fe*]X complexes, through the trends in the multinuclear NMR data, and through the Mössbauer analysis that demonstrated that the fluoride complex appeared to be exceptionally electron rich. Thus, the presence of a so-called "inverse halide order" that is the opposite of that expected on the basis of halogen electronegativities alone is firmly established.[28b,36,50,61] These experimental data appear to be consistent with the presence of Fe(d_π)−X(p_π) interactions, but the data cannot help distinguish between this interpretation

and the alternative one based on Drago's ETC bonding scheme[11] in which an ionic (electrostatic) component to the bonding may be of even greater significance than the π effect. The DFT calculations on the [Fe]X model system corroborate the "inverse halide order" of the relative electron densities at Fe, as measured by the HOMO compositions and energies as well as by the ionization potentials.

The use of thermochemical cycles based on electrode potential data establishes that all [Fe*]−X bonds under investigation are *weakened* with respect to homolytic cleavage (BDE_hom data) as a consequence of one-electron oxidation processes. In considering the Fe(d_π)−X(p_π) interactions or Drago's ETC bonding scheme, the decomposition of the BDE_hom* data into E_{elect} (electrostatic) and $E_{Pauli+orb}$ (covalent) terms seems to be most consistent with the latter interpretation, i.e., electrostatic effects are of greater significance to explain the trends than are Fe-(d_π)−X(p_π) interactions, at least in this system. For the heterolytic cleavage, in which X is cleaved as X⁻ (BDE_het data), an oxidatively induced bond strengthening is seen, experimentally and by calculations. This effect originates primarily in electrostatic effects.

The IR $\nu_{Fe−X}$ data show a shift to higher frequencies when Cp*Fe(dppe)H and Cp*Fe(dppe)Cl are oxidized to the respective 17-electron cation radicals. These results are confirmed by calculations for CpFe(dpe)H and CpFe(dpe)Cl. The IR trend is apparently at odds with the observed homolytic BDE_hom *weakening* that results, by experiment (electrochemistry derived data) and theory (DFT calculations), upon one-electron oxidation. Interestingly, for the Cp*W(dppe)H₃ complex, theory (DFT calculations on the CpW(dpe)H₃ model) and IR spectroscopic data suggest that one-electron oxidation causes a W−H bond *strengthening*.[21] Unfortunately, corresponding electrochemistry data are not available for the W system. From simple theory, it is commonly considered that the vibrational frequency correlates directly with the bond energy and inversely with the bond length.[64] The data presented by us suggest that extreme caution should be exerted when relative *homolytic* bond strengths are discussed on the basis of rather small differences in IR stretching frequencies. In this respect, we point out that the oxidatively induced increase in IR $\nu_{Fe−X}$ frequencies correlate nicely with the increase in *heterolytic* bond energies (BDE_het data). Analogous observations and conclusions have been made in recent studies of M−H bonding and IR $\nu_{M−H}$ data of Ni complexes by DuBois and co-workers.[15b]

Experimental Section

General. All manipulations were carried out under an argon atmosphere using Schlenk techniques or in Vacuum Atmospheres or Jacomex 532 dryboxes filled with nitrogen. Reagent grade ether, THF, and pentane were dried and distilled from sodium benzophenone ketyl prior to use. Dichloromethane was distilled from P₂O₅. Complexes Cp*Fe(dppe)H, Cp*Fe(dppe)H⁺PF₆⁻, Cp*Fe(dppe)Me, Cp*Fe(dppe)-Me⁺BF₄⁻, Cp*Fe(dppe)Cl, Cp*Fe(dppe)Cl⁺PF₆⁻, Cp*Fe(dppe)I, and Cp*Fe(dppe)⁺PF₆⁻ were prepared following published procedures,[19,25e] and other chemicals were purchased from commercial sources and used as received.

NMR spectra were recorded on a multinuclear Bruker DPX 200 spectrometer at 297 K. ¹H NMR spectra were recorded at 200 MHz, and all chemical shifts are reported in ppm using internal tetramethylsilane (TMS) or the residual proton resonance resulting from incomplete deuteration of the NMR solvent as the reference. ¹³C NMR spectra were recorded at 50 MHz, and all chemical shifts are reported in ppm using the carbon on the deuterated NMR solvent as the

(64) *Infrared and Raman Spectroscopy: Methods and Applications*; Schrader, B., Ed.; VCH: Weinheim, Germany, 1995; p 693.

reference. $^{31}P\{^1H\}$ NMR spectra were recorded at 81 MHz, and all chemical shifts are reported in ppm relative to external 85% H_3PO_4. ^{19}F NMR spectra were recorded at 188 MHz, and all chemical shifts are reported in ppm relative to external $CFCl_3$. Magnetic susceptibility measurements were performed in solution according to Evans' method.[37]

X-Band ESR spectra were recorded on a Bruker ESP-300E spectrometer at 77 K in liquid nitrogen. The ^{57}Fe Mössbauer spectra were recorded with a 2.5×10^{-2} C (9.25×10^8 Bq) ^{57}Co source using a symmetric triangular sweep mode.[65] Computer fitting of the Mössbauer data to Lorentzian line shapes was carried out with a previously reported computer program.[66] The isomer shift values are reported relative to iron foil at 298 K and are not corrected for the temperature-dependent second-order Doppler shift.

Infrared spectra were recorded using a Bruker instrument IFS28 ($4000-400$ cm^{-1}), a Perkin-Elmer 684 dispersive instrument ($600-200$ cm^{-1}), or a Perkin-Elmer Paragon 1000 FTIR spectrometer (KBr beam splitter, 400 cm^{-1} cutoff) with a resolution of 2 cm^{-1}. The spectra of $1-4$ and the corresponding cation PF_6^- salts were obtained as Nujol mulls between polyethylene sheets.

Cyclic voltammograms were recorded using a an EG&G-PAR model 263 potentiostat/galvanostat. The working electrode was a Pt disk electrode ($d = 0.4$ or 1.0 mm), the counter electrode was a Pt wire, and the saturated calomel electrode (SCE) or a Ag/Ag$^+$(MeCN) electrode were used as reference electrodes. The $Cp_2Fe^{0/+}$ couple was used as an internal calibrant for the potential measurements.[67] Elemental analyses were performed at the Center for Microanalyses of the CNRS at Vernaison, France.

Preparation of Cp*Fe(dppe)F (1). Method 1: From Cp*Fe-(dppe)$^+$PF$_6^-$. A dry, solid sample of CsF (0.304 g, 2.0 mmol) was added to an orange THF solution (40 mL) of Cp*Fe(dppe)$^+$PF$_6^-$ (1.660 g, 2.26 mmol) at ambient temperature. The reaction mixture turned progressively yellowish green after being stirred overnight. The solvent was removed under vacuum, and the remaining residue was extracted with ether (3×30 mL). The combined extracts were evaporated to dryness, and an 86% yield (1.050 g) of crude Cp*Fe(dppe)F was isolated as a yellowish-green, air-sensitive powder.

Method 2: From Cp*Fe(dppe)F$^+$PF$_6^-$. A sample of Cp$_2$Co (0.166 g, 0.88 mmol) was quickly added under argon to a cooled (-100 °C) red THF solution (40 mL) of Cp*Fe(dppe)F$^+$PF$_6^-$ (0.780 g, 1.03 mmol), prepared as described below. The resulting mixture was stirred while being allowed to warm slowly overnight to room temperature. The color progressively turned yellowish green. Workup provided Cp*Fe(dppe)F (0.480 g, 90% based on Cp$_2$Co).

^1H NMR (C$_6$D$_6$) δ 1.33 (s, 15 H, C$_5$Me$_5$), 1.75, 1.84 (m, 4 H, CH$_2$), 7.00$-$7.93 (m, 20 H, Ph). ^{13}C NMR (C$_6$D$_6$) δ 10.0 (C$_5$Me$_5$, $^1J_{CH} = 132$ Hz), 29.2 (t, CH$_2$, $^1J_{CH} = 124$ Hz), 82.9 (s, C$_5$Me$_5$), 127.1$-$136.6 (m, Ph). $^{31}P\{^1H\}$ NMR (C$_6$D$_6$) δ 89.4 (d, dppe, $J_{PF} = 43$ Hz). ^{19}F NMR (C$_6$D$_6$) δ -44.4 (t, Fe$-$F, $J_{PF} = 43$ Hz).

Preparation of Cp*Fe(dppe)F$^+$PF$_6^-$ (1$^+$PF$_6^-$). Method 1: From Cp*Fe(dppe)$^+$PF$_6^-$. To a cooled (-90 °C) orange THF solution (70 mL) of Cp*Fe(dppe)$^+$PF$_6^-$ (1.10 g, 1.5 mmol) was added a solid sample of Cp$_2$Fe$^+$PF$_6^-$ (0.420 g, 1.27 mmol). The color darkened immediately and at -70 °C became dark red. Stirring was continued while the mixture was allowed to warm slowly (overnight) to room temperature. The THF had partly polymerized. The remaining solvent was evaporated under vacuum and the red gummy residue was extracted with acetone (10×60 mL). The extracts were combined and evaporated to dryness, and the dark red powder was washed with ether (3×20 mL) to remove the ferrocene. Crystallization from an acetone solution layered with pentane afforded dark red, thermally and air stable crystals of Cp*Fe(dppe)F$^+$PF$_6^-$ (0.780 g, 81% based on Cp$_2$Fe$^+$PF$_6^-$).

Method 2: From Cp*Fe(dppe)F. Treatment of a THF solution (30 mL) of freshly prepared Cp*Fe(dppe)F (0.480 g, 0.79 mmol) with a sample of Cp$_2$Fe$^+$PF$_6^-$ (0.232 g, 0.70 mmol) caused an immediate color change from green to red. The mixture was stirred for 15 min, and the solvent was removed under vacuum. The red material was washed with ether (3×30 mL). An 87% yield of Cp*Fe(dppe)F$^+$PF$_6^-$ (0.460 g) was isolated.

Anal. Calcd for C$_{36}$H$_{39}$F$_7$FeP$_3$: C, 57.39; H, 5.22; P, 12.33. Found: C, 57.30; H, 5.24; P, 12.75. μ_{eff} (CH$_2$Cl$_2$, 310 K) = 1.88 μB. Mössbauer data (80 K, mm s^{-1}): I.S. = 0.426 vs Fe; Q.S. = 0.915. ESR (9:1 THF/pentane, 77 K): $g_x = 2.419$, $g_y = 2.018$, $A_F = 60$ G, $g_z = 1.998$, $A_F = 110$ G. ^1H NMR (acetone-d_6, 323 K) δ 4.57 (s, C$_5$Me$_5$, $\omega_{1/2} = 40$ Hz), 5.64 (s, CH$_2$, $\omega_{1/2} = 30$ Hz); 213 K δ 3.23 (bs, C$_5$Me$_5$, $\omega_{1/2} = 230$ Hz), 4.72 (bs, CH$_2$, $\omega_{1/2} = 190$ Hz). ^{13}C NMR (acetone-d_6, 293 K) δ 16.2 (bs, C$_5$Me$_5$, $\omega_{1/2} = 500$ Hz), 28.5 (bs, CH$_2$), 99.7 (bs, C$_5$Me$_5$, $\omega_{1/2} = 201$ Hz), 9.7, 122.7, 124.6, 130.8, 138.3 (Ph). ^{31}P NMR (acetone-d_6, 293 K) δ -143.4 (sept., $J_{PF} = 709$ Hz, PF$_6^-$). ^{19}F NMR (CD$_2$Cl$_2$, 293 K) δ -60.0 (bs, Fe$-$F, $\omega_{1/2} = 360$ Hz), -73.1 (d, $J_{PF} = 709$ Hz, PF$_6^-$).

Preparation of Cp*Fe(dppe)Br (3). A sample of KBr (0.715 g, 6.0 mmol) was added to a green solution of Cp*Fe(dppe)Cl (3.12 g, 5.0 mmol) in dichloromethane (30 mL). The reaction mixture was stirred overnight at ambient temperature. The solution was filtered and carefully layered with pentane (100 mL). After 2 weeks, 3.00 g (yield 90%) of air and thermally stable dark-brown crystals of Cp*Fe(dppe)Br were collected. Anal. Calcd for C$_{36}$H$_{39}$BrFeP$_2$: C, 64.59; H, 5.87; P, 9.25. Found: C, 64.36; H, 5.90; P, 9.31. ^1H NMR (C$_6$D$_6$) δ 1.53 (s, 15 H, C$_5$Me$_5$), 2.03 and 2.61 (2 m, 4 H, CH$_2$), 7.10$-$8.11 (m, 20 H, Ph).^{13}C NMR (C$_6$D$_6$) δ 10.8 (q, C$_5$Me$_5$, $^1J_{CH} = 128$ Hz), 31.0 (m, CH$_2$, $^1J_{CH} = 136$ Hz), 83.6 (s, C$_5$Me$_5$), 127.7$-$140.3 (m, Ph). $^{31}P\{^1H\}$ NMR (C$_6$D$_6$) δ 93.2 (s, dppe).

Preparation of Cp*Fe(dppe)Br$^+$PF$_6^-$ (3$^+$PF$_6^-$). A sample of Cp$_2$Fe$^+$PF$_6^-$ (0.298 g, 0.9 mmol) was added to a dark-orange solution of Cp*Fe(dppe)Br (0.67 g, 1.0 mmol) in THF (20 mL) and the reaction mixture was stirred for 1 h at ambient temperature. After removal of the solvent under vacuum, the dark residue was washed with ether (5×50 mL). Following crystallization from THF/pentane, 0.70 g (95% yield) of air and thermally stable black microcrystals of Cp*Fe(dppe)-Br$^+$PF$_6^-$ were isolated. Anal. Calcd for C$_{36}$H$_{39}$BrF$_6$FeP$_3$: C, 53.10; H, 4.83; P, 11.41. Found: C, 53.60; H, 4.79; P, 12.13. μ_{eff} (CD$_2$Cl$_2$, 297 K) = 2.7 μB.

Chemical Reduction of Cp*Fe(dppe)Br$^+$PF$_6^-$. At -80 °C under an atmosphere of argon, a solid sample of Cp$_2$Co (0.17 g, 0.9 mmol) was quickly added to a dark-brown solution of Cp*Fe(dppe)Br$^+$PF$_6^-$ (0.814 g, 1.0 mmol) in THF (30 mL). The mixture was stirred for 1 h. After heating to ambient temperature, the solvent was removed under vacuum and the remaining residue was extracted with ether (3×30 mL). Crystallization from dichloromethane/pentane provided 0.50 g (95% yield) of dark-brown microcrystals of Cp*Fe(dppe)Br, analyzed as above.

Preparation of Cp*Fe(dppe)I$^+$PF$_6^-$ (4$^+$PF$_6^-$). At room temperature, a sample of Cp$_2$Fe$^+$PF$_6^-$ (0.298 g, 0.9 mmol) was added to an orange-brown solution of Cp*Fe(dppe)I (0.720 g, 1.0 mmol) in THF (20 mL). The reaction mixture was stirred for 1 h and the solvent was removed under vacuum. The remaining dark solid residue was washed with ether (5×50 mL). Crystallization from THF/pentane gave 0.70 g (90% yield) of air and thermally stable black microcrystals of Cp*Fe(dppe)I$^+$PF$_6^-$. Anal. Calcd for C$_{36}$H$_{39}$F$_6$FeIP$_3$: C, 50.20; H, 4.56; P, 10.79. Found: C, 51.12; H, 4.48; P, 11.23. μ_{eff} (CD$_2$Cl$_2$, 297 K) = 2.3 μB.

Preparation of Cp*Fe(dppe)H$^+$PF$_6^-$ (5$^+$PF$_6^-$). This method is an improvement over that previously reported.[19b] At room temperature, a sample of Cp$_2$Fe$^+$PF$_6^-$ (0.298 g, 0.9 mmol) was added to an orange solution of Cp*Fe(dppe)H (0.590 g, 1.0 mmol) in THF (20 mL). The mixture was stirred for 15 min, during which the color of the solution turned progressively red. The solvent was removed under vacuum, and the remaining dark solid residue was washed with diethyl ether (5×30 mL). Crystallization from acetone/pentane mixture gave air and thermally stable red microcrystals of Cp*Fe(dppe)H$^+$PF$_6^-$ (0.75 g, 95%). Anal. Calcd for C$_{36}$H$_{40}$F$_6$FeP$_3$: C, 58.79; H, 5.48; P, 12.63. Found: C, 58.56; H, 5.31; P, 12.70. IR (Nujol) ν_{Fe-H} 1886 cm^{-1}; Mössbauer (4.2 K, mm s^{-1}) I.S. = 0.260, Q.S. = 0.840. EPR (CH$_2$-Cl$_2$/CH$_2$ClCH$_2$Cl, 77 K): $g_1 = 1.9944$, $g_2 = 2.0430$, $g_3 = 2.4487$. μ_{eff} (CH$_2$Cl$_2$, 297 K) = 2.40 μB.

(65) Varret, F.; Mariot, J.-P.; Hamon, J.-R.; Astruc, D. *Hyperfine Interact.* **1988**, *39*, 67.

(66) (a) Boinnard, D.; Boussekssou, A.; Dworkin, A.; Savariault, J.-M.; Varret, F.; Tuchagues, J.-P. *Inorg. Chem.* **1994**, *33*, 271. (b) Varret, F.; Varret, F., Ed.; *International Conference on Mössbauer Effects Applications*; Indian Science Academy, New Delhi, 1982: Jaipur, India, 1981.

(67) Connelly, N. G.; Geiger, W. E. *Chem. Rev.* **1996**, *96*, 877.

Table 11. Crystal Data, Data Collection, and Refinement Parameters for $1^+PF_6^-$, $2^+PF_6^-$, and $6^+BF_4^-$

	$1^+PF_6^-$	$2^+PF_6^-$	$6^+BF_4^-$
formula	$C_{36}H_{39}F_7FeP_3$	$C_{36}H_{39}ClF_6FeP_3$	$C_{37}H_{42}BF_4FeP_2$
fw	753.43	769.88	691.31
temperature (K)	293(2)	293(2)	293(2)
crystal system	monoclinic	orthorhombic	monoclinic
space group	$P2_1/n$	$P2_12_12_1$	$P2_1/n$
a (Å)	14.253(8)	12.763(3)	31.490(4)
b (Å)	15.252(2)	13.877(7)	9.834(4)
c (Å)	15.873(4)	19.551(7)	22.322(5)
α (deg)	90	90	90
β (deg)	90.86(3)	90	92.42(2)
γ (deg)	90	90	90
V (Å^{-3})	3450(2)	3463(2)	6906(3)
Z	4	4	4
D(calcd) (g cm^{-3})	1.450	1.477	0.665
crystal size (mm)	$0.35 \times 0.35 \times 0.20$	$0.25 \times 0.25 \times 0.12$	$0.65 \times 0.45 \times 0.45$
$F(000)$	1556	1588	1444
diffractometer	CAD4	CAD4	CAD4
radiation	MoK$_\alpha$	MoK$_\alpha$	MoK$_\alpha$
abs coef (mm^{-1})	0.640	0.710	0.288
θ range (deg)	1.85−24.98	1.80−24.95	1.10−24.98
range h ,k, l	0/16, 0/18, −18/18	0/15, 0/16, 0/23	−37/37, 0/10, 0/26
total no. of reflcns	6297	3406	11859
no. of unique reflcns	6040	3406	11553
no. of obsd reflcns [$I > 2\sigma(I)$]	3424	2423	6598
no. of restraints/no. of parameters	0/425	0/419	0/775
w = $1/[\sigma^2(F_o)^2 + (aP)^2 + bP]$	$a = 0.0845$	$a = 0.1374$	$a = 0.1540$
(where $P = [F_o^2 + F_c^2]/3$)	$b = 1.2816$	$b = 0.0000$	$b = 15.9595$
final R	0.0476	0.0530	0.0757
R_w	0.1284	0.1453	0.2241
R indices (all data)	0.1329	0.1024	0.1651
R_w (all data)	0.1540	0.1770	0.2836
goodness of fit/F^2	1.030	1.006	1.066
largest diff peak	0.568	0.736	1.165
and hole (e Å^{-3})	−0.417	−0.535	−0.775

Chemical Reduction of Cp*Fe(dppe)I$^+$PF$_6^-$. Following the same procedure and workup as described above for the bromo derivative, Cp*Fe(dppe)I$^+$PF$_6^-$ (0.86 g, 1.0 mmol) was treated with Cp$_2$Co (0.17 g, 0.9 mmol) to provide 0.610 g (95%) of Cp*Fe(dppe)I after crystallization from dichloromethane/pentane.

X-ray Crystallographic Studies of Cp*Fe(dppe)F$^+$PF$_6^-$, Cp*Fe-(dppe)Cl$^+$PF$_6^-$, and Cp*Fe(dppe)Me$^+$BF$_4^-$. X-ray quality crystals of Cp*Fe(dppe)Cl$^+$PF$_6^-$ were obtained after 3 weeks from a concentrated dichloromethane solution that was layered with pentane. Crystals of Cp*Fe(dppe)Me$^+$BF$_4^-$ were grown from a concentrated THF solution that was layered with pentane, and crystals of Cp*Fe(dppe)F$^+$PF$_6^-$ were grown from acetone−pentane. A summary of the crystallographic data is given in Table 11. Complete details of the crystal data, X-ray data collection, and structure solution are provided as Supporting Information. Cell constants and orientation matrix for data collection were obtained from a least-squares refinement using 25 high-θ reflections. For all compounds, after Lorenz and polarization corrections,[68] the structures were solved with SIR-97,[69] which revealed many non-hydrogen atoms of the molecules. After anisotropic refinements, a Fourier difference map revealed many hydrogen atoms. The whole structures were next refined with SHELXL97,[70] by the full-matrix least-squares techniques (use of F^2 magnitude; x, y, z, β_{ij} for Fe, P, Cl, F, and C atoms, and x, y, z in riding mode for H atoms with variables (N(var.)), observations and "ω" used as defined in Table 11). Atomic scattering factors were taken from the literature.[71] A Silicon Graphics Indy computer with the MOLEN package (ENRAF-NONIUS, 1990)

was used for structure determination.[72] ORTEP views of $1^+PF_6^-$, $2^+PF_6^-$, and $6^+BF_4^-$ were generated with PLATON98.[73] All the calculations were performed on a Pentium NT Server computer.

Computational Details. DFT calculations[74] were carried out using the Amsterdam Density Functional (ADF) program.[75] The model compounds CpFe(dpe)X,[17] to be abbreviated as [Fe]X,[17] were used to reduce computational effort. The Vosko−Wilk−Nusair parametrization[76] was used to treat electron correlation within the local density approximation (LDA). The nonlocal corrections of Becke[77] and of Perdew[78] were added to the exchange and correlation energies, respectively. The numerical integration procedure applied for the calculations was developed by te Velde et al.[74] A triple-ζ Slater-type orbital (STO) basis set was used for Fe 3d and 4s, and a single-ζ STO was used for Fe 4p. Concerning X (X = F, Cl, Br, I, CH$_3$, H), a triple-ζ STO basis set was employed for H 1s, C 2s and 2p, F 2s and 2p, Cl 3s and 3p, Br 3d, 4s, and 4p, and I 4d, 5s, and 5p, augmented with a single-ζ polarization function (2p for H; 3d for C, F, and Cl; and 4d for Br). The other atoms were described by a double-ζ STO basis set for H 1s, C 2s and 2p, and P 3s and 3p, augmented with a single-ζ polarization function (2p for H and C; 3d for P). Full geometry optimizations (assuming C_1 symmetry) were carried out on each complex, using the analytical gradient method implemented by Verluis

(68) Spek, A. L. *HELENA. Program for the handling of CAD4-Diffractometer Output SHELX(S/L)*; Utrecht University: Utrecht, The Netherlands, 1997.

(69) Altomare, A.; Burla, M. C.; Camalli, M.; Cascarano, G.; Giacovazzo, C.; Guagliardi, A.; Moliterni, A. G. G.; Polidori, G.; Spagna, R. *J. Appl. Chem.* **1998**, *31*, 74.

(70) Sheldrick, G. M. *SHELX97. Program for the Refinement of Crystal Structures*; University of Göttingen: Göttingen, Germany, 1997.

(71) *International Tables for X-ray Crystallography*; Kluwer Academic Publishers: Dordrecht, The Netherlands, 1992; Vol. C.

(72) Fair, C. K. *MolEN. An Interactive Intelligent System for Crystal Structure Analysis*; ENRAF-NONIUS: Delft, The Netherlands, 1990.

(73) Spek, A. L. *PLATON-98, A Multipurpose Crystallographic Tool*; Utrecht University: Utrecht, The Netherlands, 1998.

(74) (a) Baerends, E. J.; Ellis, D. E.; Ros, P. *Chem. Phys.* **1973**, *2*, 41. (b) Baerends, E. J.; Ros, P. *Int. J. Quantum Chem.* **1978**, *S12*, 169. (c) Boerrigter, P. M.; te Velde, G.; Baerends, E. J. *Int. J. Quantum Chem.* **1988**, *33*, 87. (d) te Velde, G.; Baerends, E. J. *J. Comput. Phys.* **1992**, *99*, 84.

(75) Amsterdam Density Functional (ADF) program, version 2.3; Vrije Universiteit: Amsterdam, The Netherlands, 1996.

(76) Vosko, S. D.; Wilk, L.; Nusair, M. *Can. J. Chem.* **1990**, *58*, 1200.

(77) Becke, A. D. *J. Chem. Phys.* **1986**, *84*, 4524. Becke, A. D. *Phys. Rev. A.* **1988**, *38*, 3098.

(78) Perdew, J. P. *Phys. Rev. B* **1986**, *33*, 8882; *34*, 7406.

and Ziegler.[79] Spin-unrestricted calculations were performed for all open-shell systems considered.

Diabatic ionization potentials were calculated as the energy difference between the optimized geometries of the reduced and oxidized species. The computed BDE values correspond to the following reactions: $CpFe(dpe)X \rightarrow CpFe(dpe) + X$ and $CpFe(dpe)X^+ \rightarrow CpFe(dpe)^+ + X$ (homolytic dissociation, BDE_{hom}); $CpFe(dpe)X \rightarrow CpFe(dpe)^+ + X^-$ and $CpFe(dpe)X^+ \rightarrow CpFe(dpe)^{2+} + X^-$ (heterolytic dissociation, BDE_{het}). These have been calculated by subtracting the energies of the dissociated species from those of the corresponding $CpFe(dpe)X^{0/+}$ complexes. The considered energies were those obtained after full geometry optimizations, i.e., including the fragment geometrical relaxation. The Basis Set Superposition Errors (BSSE) were evaluated by using the counterpoise method.[80] The organometallic fragments $CpFe(dpe)$, $CpFe(dpe)^+$, and $CpFe(dpe)^{2+}$ were considered in their ground state (i.e. doublet, triplet, and doublet state, respectively).[55]

(79) Verluis, L.; Ziegler, T. *J. Chem. Phys.* **1988**, *88*, 322.

(80) (a) van Duijneveldt, F. B.; van Duijneveldt de Rijdt, J. G. C. M.; van Lenthe, J. H. *Chem. Rev.* **1994**, *94*, 1873. (b) Boys, S. F.; Bernardi, F. *Mol. Phys.* **1970**, *19*, 553. (c) Rosa, A.; Ehlers, A. W.; Baerends, E. J.; Snijders, J. G.; te Velde, G. *J. Phys. Chem.* **1996**, *100*, 5690.

Supporting Information Available: X-ray crystallographic file (CIF) with listings of crystal data, X-ray experimental details, atomic coordinates, thermal parameters, and bond distances and angles for $\mathbf{1}^+PF_6^-$, $\mathbf{2}^+PF_6^-$, and $\mathbf{6}^+BF_4^-$. This material is available free of charge via the Internet at http://pubs.acs.org.

JA0106927